Supplementary Information (SI) for Chemical Communications.
This journal is © The Royal Society of Chemistry 2025

Electronic Supplementary Information

Octacyano-substituted tridecacyclene: A non-benzenoid cyanocarbon with low-lying LUMO and multistage redox properties

Erik Misselwitz, Jonas Spengler, Frank Rominger, and Milan Kivala*

[*] E. Misselwitz, J. Spengler, Dr. F. Rominger, Prof. Dr. M. Kivala
Organisch-Chemisches Institut, Universität Heidelberg
Im Neuenheimer Feld 270, 69120 Heidelberg (Germany)
E-mail: milan.kivala@oci.uni-heidelberg.de

Table of Contents

1. Experimental Details

General

All solvents and reagents were purchased at reagent grade from commercial suppliers (Merck/Sigma-Aldrich, TCI, Thermo Fisher Scientific, Acros Organics, Honeywell, BLD Pharmatech) and used without additional purification. Dry tetrahydrofuran (THF) was obtained by distillation over sodium metal. Complete dryness was indicated by the dark blue color of the benzophenone ketyl radical anion. For usage in the glovebox, THF was degassed using the freeze-pump-thaw method, transferred to the glovebox without exposure to air and stored over activated molecular sieves. All reactions involving oxygen- or moisture-sensitive compounds were performed in heat gun dried glassware under an atmosphere of nitrogen using standard *Schlenk* techniques. The addition of oxygen- and moisture-sensitive solvents and reagents was carried out using nitrogen-flushed stainless-steel cannulas and plastic syringes. Thin layer chromatography was monitored on ALUGRAM aluminum plates from Macherey-Nagel, coated with 0.20 mm SiO_2, by irradiation with UV-light (λ= 365 and 254 nm). Flash column chromatography was carried out with SiO_2 from Macherey-Nagel (technical grade 60 M, pore size 60 Å, 40−63 µm particle size).

Instruments used

Nuclear Magnetic Resonance. Spectra were recorded at room temperature (295 K) on a Bruker Avance III 300, 400, 500, 600 or 700 at the Institute of Organic Chemistry (Heidelberg University). Proton broad band decoupling was applied for ^{13}C measurements. Deuterated solvents were used as purchased from Merck/Sigma-Aldrich or Deutero GmbH. Chemical shifts (reported in parts per million ppm) were referenced[1] to δ_H = 7.26 ppm ($CDCl_3$), 2.50 ppm (DMSO-d_6) and 5.91 ppm (TCE-d_2) for ^1H and δ_C = 77.16 ppm ($CDCl_3$), 39.52 ppm (DMSO-d_6) and 74.2 ppm (TCE-d_2) for ^{13}C and interpreted with MestReNova Version 14.1.2-25024. 1,1,2,2-tetrachloroethane-d_2 is abbreviated as TCE-d_2 and dimethyl sulfoxide-d_6 is abbreviated as DMSO-d_6. Apparent multiplicity is reported as s (singlet), d (doublet), dd (doublet of doublets), t (triplet), or m (multiplet).

Mass Spectrometry. Mass spectra and high-resolution mass spectra (MS/HRMS) were recorded at the Institute of Organic Chemistry (Heidelberg University). Matrix-assisted laser desorption/ionization (MALDI) and laser desorption/ionization (LDI) spectra were measured on a Bruker ApexQe hybrid 9.4 FT-ICR spectrometer or Bruker AutoFlex Speed time-of-flight spectrometer. DCTB (*trans*-2-[3-(4-*tert*-butylphenyl)2-methyl-2-propenylidene]malononitrile) was used as a matrix for the MALDI-MS experiments. Electron Ionization (EI) spectra were recorded on a JEOL AccuTOF GCx spectrometer.

Absorption Spectra. UV-Vis spectra were recorded on an Agilent Cary 60 UV-Vis spectrometer and measured in CH_2Cl_2 in the wavelength region of 230 to 800 nm under ambient conditions (rt: room temperature). UV-Vis-NIR spectra were measured on an Agilent Cary 5000 UV/Vis-NIR spectrometer in THF in the wavelength region of 230 to 2200 nm in a sealable quartz glass cell (10x10 mm) manufactured by Hellma Analytics under N_2 atmosphere at rt. The abbreviation br. (broad) sh. (shoulder) refers to saddle points or shoulders in the absorption spectrum. The data obtained was interpreted with Spectra Manager from JASCO.

X-ray Crystallography. Single crystals were obtained by slow gas phase diffusion under the given conditions. The Bruker APEX-II Quazar diffractometer (radiation MoKα, λ = 0.71073 Å) with a CCD area detector and the STOE Stadivari instrument (radiation CuKα, λ=1.54178 Å) with a Pilatus CCD area detector (0.5° ω-scans) were used for

data collection by the X-ray crystallography department at the Institute of Organic Chemistry (Heidelberg University). Structures were solved with the ShelXT[2] structure solution program and refined against F2 with a full-matrix least-squares algorithm with ShelXL.[3] Hydrogen atoms were treated with riding models. Graphic visualization and measurement of torsion angles were done with Mercury 2020.1.[4]

Cyclic, Differential Pulse and Square Wave Voltammetry. A BASi Cell Stand instrument with a glassy carbon disk working electrode (3.0 mm diameter), an Ag/AgCl (3 M NaCl) quasi-reference electrode, and a platinum wire auxiliary electrode were used to record cyclic, differential pulse and square wave voltammograms. Measurements were conducted in 0.1 M electrolyte solutions of *n*-Bu_4NPF_6 (used without further purification) in anhydrous 1,2-dichlorobenzene (*o*-DCB)/MeCN 4:1 (v/v) or CH_2Cl_2 which had been degassed by bubbling nitrogen through the solution for 30 min. The respective compounds were measured at a scan rate of 149 mV s^{-1}, followed by the addition of ferrocene as the internal standard and re-measurement.

Spectroelectrochemistry. UV-Vis-NIR spectroelectrochemical experiments were carried out using an airtight optically transparent thin-layer electrochemical (OTTLE) cell.[5] The cell was equipped with a platinum minigrid (32 wires per cm) working and auxiliary electrodes, an Ag microwire pseudoreference electrode, and an optically transparent CaF_2 window. The potential during the spectroelectrochemical experiment was controlled using a BASi Epsilon EClipse potentiostat and the spectral changes were monitored using an Agilent Cary 5000 UV/Vis-NIR spectrometer. Measurements were conducted at rt in 0.1 M electrolyte solutions of *n*-Bu_4NPF_6 (used without further purification) in anhydrous CH_2Cl_2 which had been degassed by bubbling nitrogen through the solution for 30 min. The respective potential was held for 5 minutes before recording each spectrum.

Infrared Spectroscopy. A JASCO FT/IR-4600 FTIR spectrometer was operated in ATR mode to record infrared spectra. The respective transmission spectra are baseline corrected, depicted in cm^{-1} and labeled according to the following abbreviations: s (strong), m (medium), w (weak).

Melting Point. The melting point was determined on a Büchi M-560 melting point apparatus in open capillaries. Decomp. refers to decomposition.

IUPAC Names and Formulas. IUPAC names and numbering of the synthesized compounds were generated using ACD/Labs 2021.

High-Performance Liquid Chromatography. High-performance liquid chromatography (HPLC) was performed on a setup from Shimadzu consisting of a LC20-AP preparative pump, a DGU-405 degassing unit, a CTO-40C column oven, an SPD-M40 diode array detector, an FCV-20AH_2 valve unit, an FRC-10A fraction collector and an CBM-20A communication bus module. On the analytical scale, a Macherey-Nagel 5 µm (250 x 4.60 mm) normal phase column equipped with a column protection system and a Macherey-Nagel 5 µm (3 mm x 4 mm) precolumn was used. On the preparative scale, a Macherey-Nagel 5 µm (250 x 21 mm) normal phase column equipped with a column protection system and a Macherey-Nagel 5 µm (10 mm x 16 mm) precolumn was employed.

Computational Details. Quantum chemical calculations were performed using the Gaussian 16 program package.[6] Ground state geometry optimizations were performed by employing the B3LYP[7] functional, the 6-311+G(d,p)[8] basis set and Grimme's D3 dispersion correction[9] with BJ-damping.[10] Thereby, ultra-tight convergence criteria of the respective computational method were used. Frequency calculations at the same level of theory were employed to verify the geometries as local minima possessing no imaginary frequencies. Exited state calculations were carried out within the time-dependent (TD) DFT approximation, using the CAM-B3LYP[11] functional with the same basis-set and dispersion correction as above alongside the polarizable continuum model (PCM)[12] for

solvation using dichloromethane or tetrahydrofuran parameters. For every compound, the energetically lowest 50 excited states were calculated. A linewidth of 0.2 eV was assumed for the predicted UV-Vis-NIR spectra using the Gaussview 6 software.[13] Calculations on open-shell species were performed within the spin-unrestricted Kohn-Sham DFT formalism. The stability of the wavefunction generated by the self-consistent filed (SCF) calculation was tested by using the “stable” keyword in Gaussian 16. Nucleus independent chemical shifts (NICS) were calculated using the Gauge-Independent Atomic Orbital (GIAO)[14,15] approach, as implemented in Gaussian 16 at the GIAO-B3LYP(D3BJ)/6-311+G(d,p) level of theory. Analysis of the results was done with the Multiwfn 3.8 software.[16]

1. Synthesis

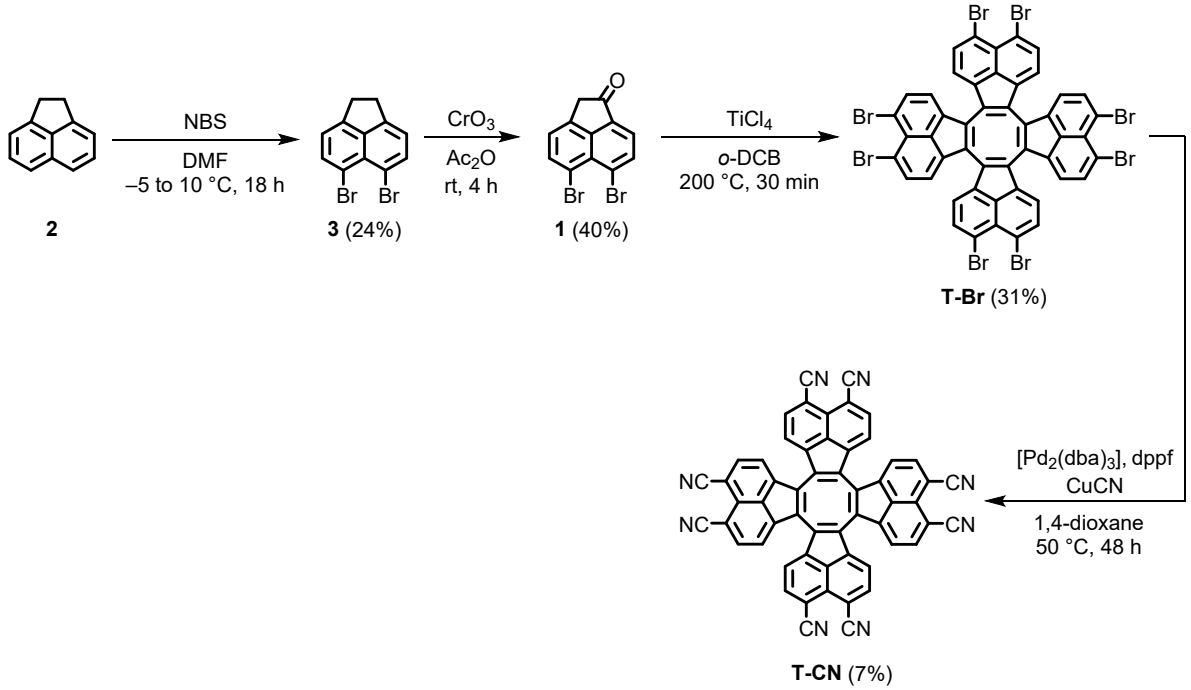

Scheme S1. Synthetic pathway towards octacyano-substituted tridecacyclene **T-CN**. NBS = *N*-bromosuccinimide, DMF = *N*,*N*-dimethylformamide, *o*-DCB = 1,2-dichlorobenzene, dba = dibenzylideneacetone, dppf = 1,1`-bis(diphenylphosphino)ferrocene.

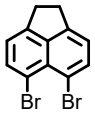

3

5,6-Dibromo-1,2-dihydroacenaphthylene (3). 1,2-Dihydroacenaphthylene (**2**) (170 g, 1.12 mol) was suspended in DMF (459 mL) and the mixture was cooled to 0 °C. *N*-Bromosuccinimide (425 g, 7.47 mol) was added in five portions over a period of 5 h. The resulting suspension was stirred at 10 °C for 18 h whereupon a precipitate formed. The precipitate was filtered and washed with ethanol (800 mL) until the filtrate was colorless. The crude product was recrystallized from hot $CHCl_3$ yielding compound **3** (82.5 g, 24%) as a colorless solid.

M.p.: 173−174 °C (lit. 173–175 °C).

Rf = 0.40 (SiO_2, petroleum ether).

^{1}H NMR (400 MHz, $CDCl_3$): δ = 7.80 (d, *J* = 7.5 Hz, 2H), 7.10 (d, *J* = 7.4 Hz, 2H), 3.31 (s, 4H) ppm.

^{13}C NMR (101 MHz, $CDCl_3$): δ = 147.2, 142.1, 136.0, 128.0, 121.1, 114.5, 30.2 ppm.

EI-HRMS: m/z calcd. for $C_{12}H_8{}^{79}Br_2$ $[M]^+$: 309.8993; found: 309.8992.

Analytical data are consistent with those reported in the literature.[17]

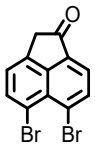

1

5,6-Dibromoacenaphthylen-1(2*H*)-one (1). 5,6-dibromo-1,2-dihydroacenaphthylene (**3**) (6.00 g, 19.2 mmol) was suspended in acetic anhydride (396 mL) and gently heated until the material was almost fully dissolved. Upon cooling to room temperature, CrO_3 (2.88 g, 28.9 mmol) was added in three portions over 1 h. The reaction mixture was stirred at room temperature for 4 h, whereupon its color changed from pale yellow to dark green. Subsequently, the mixture was poured onto ice. Upon melting of the ice, the mixture was extracted with CH_2Cl_2 (3 × 300 mL). The combined organic phases were dried over Na_2SO_4, filtered and the solvents were removed under reduced pressure. The crude product was evaporated onto Celite and subsequently subjected to flash column chromatography (SiO_2, petroleum ether/CH_2Cl_2 1:1) yielding compound **1** (2.48 g, 40%) as a colorless solid.

M.p.: 229−230 °C

R_f = 0.45 (SiO_2, petroleum ether/CH_2Cl_2 1:1).

^{1}H NMR (400 MHz, $CDCl_3$): δ = 8.10 (d, J = 7.5 Hz, 1H), 7.98 (d, J = 7.4 Hz, 1H), 7.74 (d, J = 7.5 Hz, 1H), 7.30 (d, J = 7.4 Hz, 1H), 3.76 (d, J = 1.1 Hz, 2H) ppm.

^{13}C NMR (101 MHz, $CDCl_3$): δ = 200.9, 145.0, 136.7, 136.4, 135.8, 135.4, 128.0, 126.3, 122.9, 122.5, 117.0, 41.6 ppm.

IR (FT-ATR): $\tilde{\nu}$ = 3072 (w), 2922 (br m), 2851 (w), 1710 (s), 1600 (m), 1554 (m), 1480 (m), 1414 (m), 1382 (m), 1324 (m), 1202 (m), 1140 (m), 1103 (m), 1020 (s), 984 (m), 819 (m), 704 (w), 644 (m), 609 (m), 558 (m), 516 (m) cm^{-1}.

UV-Vis (CH_2Cl_2): λ_{max} (ε) = 255 (20200), 334 (6000), 354 (6600) nm (L mol^{-1} cm^{-1}).

EI-HRMS: *m/z* calcd. for $C_{12}H_6O^{79}Br_2$ $[M]^+$: 323.8779; found: 323.8781.

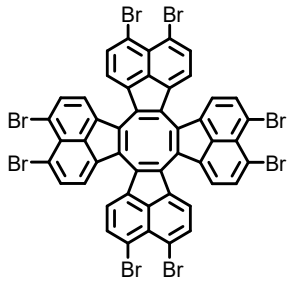

T-Br

1,6,7,12,13,18,19,24-Octabromocycloocta[1,2-*a*:3,4-*a′*:5,6-*a″*:7,8-*a‴*]tetraacenaphthylene (T-Br). In a three-neck flask equipped with an N_2-inlet, a condenser and a rubber septum, $TiCl_4$ (8.73 g, 5.04 mL, 46.0 mmol) was mixed with 1,2-dichlorobenzene (56.2 mL) under an atmosphere of nitrogen, and the mixture was heated to 200 °C. In a separate vessel, 5,6-dibromoacenaphthylen-1(2*H*)-one (**5**) (2.50 g, 7.67 mmol) was suspended in 1,2-dichlorobenzene (56.2 ml) and gently heated until fully dissolved. The solution of **5** was then added to the refluxing solution of $TiCl_4$ dropwise over the course of 10 min. After stirring at 200 °C for 20 min, the hot reaction mixture was slowly poured into an ice/conc. HCl (56.2 mL) mixture. Upon melting of the ice, the phases were separated, and the aq. phase was extracted with toluene (4 × 300 mL). The combined organic phases were dried over Na_2SO_4, filtered and the solvents were removed under reduced pressure. Twofold recrystallization of the crude product from hot toluene afforded compound **T-Br** (730 mg, 31%) as a dark brown solid.

M.p.: > 400 °C.

^{1}H NMR (700 MHz, TCE-d_2, 393 K): δ = 7.98 (d, J = 7.5 Hz, 8H), 7.40 (d, J = 7.5 Hz, 8H) ppm.

^{13}C NMR (176 MHz, TCE-d_2, 393 K): δ =140.3, 136.5, 135.6, 132.4, 126.2, 125.6, 122.1 ppm.

IR (FT-ATR): $\tilde{\nu}$ = 3066 (w), 3037 (w), 2358 (w), 1877 (w), 1570 (m), 1465 (m), 1408 (s), 1200 (m), 1088 (m), 1029 (s), 888 (m), 826 (s) cm^{-1}.

UV-Vis (CH_2Cl_2): λ_{max} (ε) = 315 (17600), 367 (35900), 383 (42800), 429 (22700), 446 (20900) nm (L mol^{-1} cm^{-1}).

LDI-HRMS: *m/z* calcd. for $C_{48}H_{16}{}^{79}Br_8$ [M]$^+$: 1223.4719; found: 1223.4700.

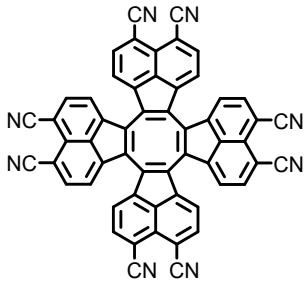

T-CN

Cycloocta[1,2-*a*:3,4-*a*':5,6-*a*'':7,8-*a*''']tetraacenaphthylen-1,6,7,12,13,18,19,24-octacarbonitrile (T-CN). Dry 1,4-dioxane was deoxygenated by bubbling with nitrogen for 30 min. Meanwhile, a dry Schlenk tube was charged with brominated tetramer **T-Br** (50.0 mg, 40.6 µmol), CuCN (900 mg, 10.1 mmol), [$Pd_2(dba)_3$] (7.43 mg, 8.12 µmol) and 1,1'-bis(diphenylphosphino)ferrocene (18.0 mg, 32.5 µmol). The reaction vessel was evacuated and refilled with nitrogen in three cycles. The deoxygenated dry 1,4-dioxane (5 mL) was added and the mixture was stirred at 50 °C for 48 h. Upon cooling to rt, the reaction mixture was diluted with CH_2Cl_2 (15 mL) and filtered through a pad of Celite, which was rinsed with CH_2Cl_2 (100 mL). The solvents were removed under reduced pressure. The crude product was purified via column chromatography (SiO_2, CH_2Cl_2/MeOH 100:1) followed by recycling high performance liquid chromatography (NP, CH_2Cl_2/MeOH 100:1, 15 mL/min) to afford the title compound **T-CN** (2.12 mg, 7%) as a brown solid.

M.p.: >400 °C.

R_f = 0.21 (SiO_2, CH_2Cl_2/MeOH 100:1).

HPLC: t_R = 4.65 min (SiO_2, 250 x 21 mm, flow = 20 mL min^{-1}, CH_2Cl_2/MeOH 100:1).

^{1}H NMR (700 MHz, DMSO-d_6, 393 K): δ = 8.36 (d, J = 7.3 Hz, 8H), 7.86 (d, J = 7.3 Hz, 8H) ppm.

^{13}C NMR (176 MHz, DMSO-d_6, 393 K) δ = 142.3, 139.0, 138.4, 128.4, 125.7, 123.3, 115.0, 107.6 ppm.

IR (FT-ATR) $\tilde{\nu}$ = 2952 (s), 2923 (s), 2852 (s), 2223 (m), 2162 (w), 1732 (m), 1699 (w), 1606 (w), 1456 (m), 1442 (m), 1376 (w), 1259 (m), 1144 (w), 1094 (m), 1020 (m), 846 (m), 797 (m), 679 (w) cm^{-1}.

UV-Vis: (CH_2Cl_2, rt) λ_{max} (ε) =262 (36500), 293 (19200), 362 (39500), 378 (38200), 431 (12100), 457 (10300) nm (L mol^{-1} cm^{-1}).

MALDI-HRMS (DCTB): *m/z* calcd. for $C_{56}H_{16}N_8$ $[M]^-$: 800.1498; found: 800.1519.

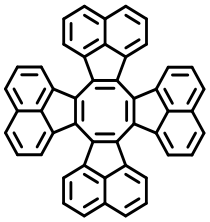

T

Cycloocta[1,2-*a*:3,4-*a′*:5,6-*a″*:7,8-*a‴*]tetraacenaphthylene (T). Compound **T** was prepared according to a literature procedure.[18] In a three-neck flask equipped with an N_2-inlet, a condenser and a rubber septum, $TiCl_4$ (2.03 g, 1.17 mL, 10.7 mmol) was mixed with 1,2-dichlorobenzene (13.0 mL) under an atmosphere of nitrogen, and the mixture was heated to 200 °C. Meanwhile, acenaphthylen-1(2*H*)-one (300 mg, 1.78 mmol) was dissolved in 1,2-dichlorobenzene (13.0 ml). The solution of acenaphthylen-1(2*H*)-one was then added to the refluxing mixture dropwise over the course of 10 min. After stirring at 200 °C for 15 min, the hot reaction mixture was slowly poured into an ice/conc. HCl (13 mL) mixture. Upon melting of the ice, the phases were separated, and the aq. phase was extracted with CH_2Cl_2 (3 × 100 mL). The combined organic phases were dried over Na_2SO_4, filtered and the solvents were removed under reduced pressure. The crude product was evaporated onto Celite and subsequently subjected to flash column chromatography (SiO_2, petroleum ether/CH_2Cl_2 5:1 to 4:1) to give the title compound **T** (50 mg, 21%) as a dark brown solid.

M.p.: > 400 °C.

^{1}H NMR (700 MHz, $CDCl_3$, rt): δ = 7.87 (d, J = 8.1 Hz, 8H), 7.68 (d, J = 6.9 Hz, 8H), 7.57 (dd, J = 8.1, 6.9 Hz, 8H) ppm.

^{13}C NMR (176 MHz, $CDCl_3$, rt): δ = 139.6, 136.7, 128.9, 127.2, 126.7, 126.4, 124.0 ppm.

MALDI-HRMS: *m/z* calcd. for $C_{48}H_{24}$ $[M]^+$: 600.1873; found: 600.1871.

Analytical data are consistent with those reported in literature.[18]

2. NMR Data

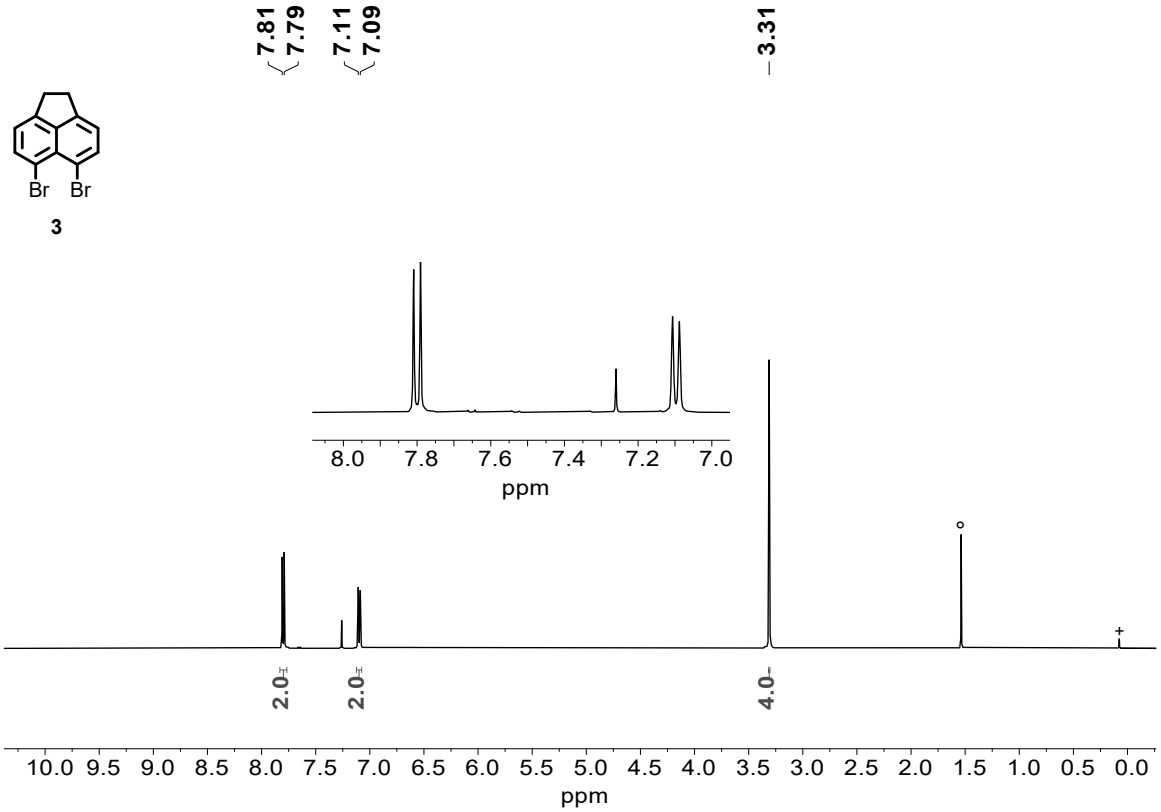

Figure S1. ^{1}H NMR spectrum of **3** (400 MHz, $CDCl_3$, rt), ° H_2O, + silicone grease.

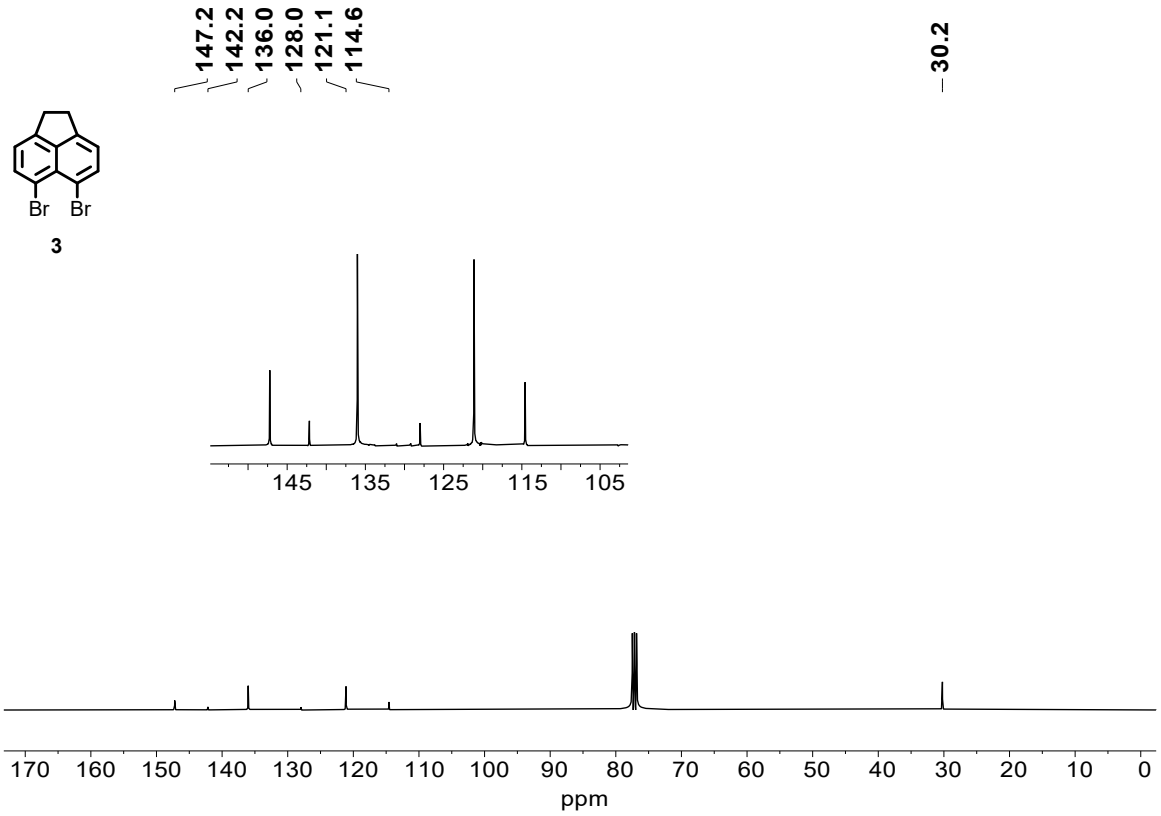

Figure S2. ^{13}C NMR spectrum of **3** (101 MHz, $CDCl_3$, rt).

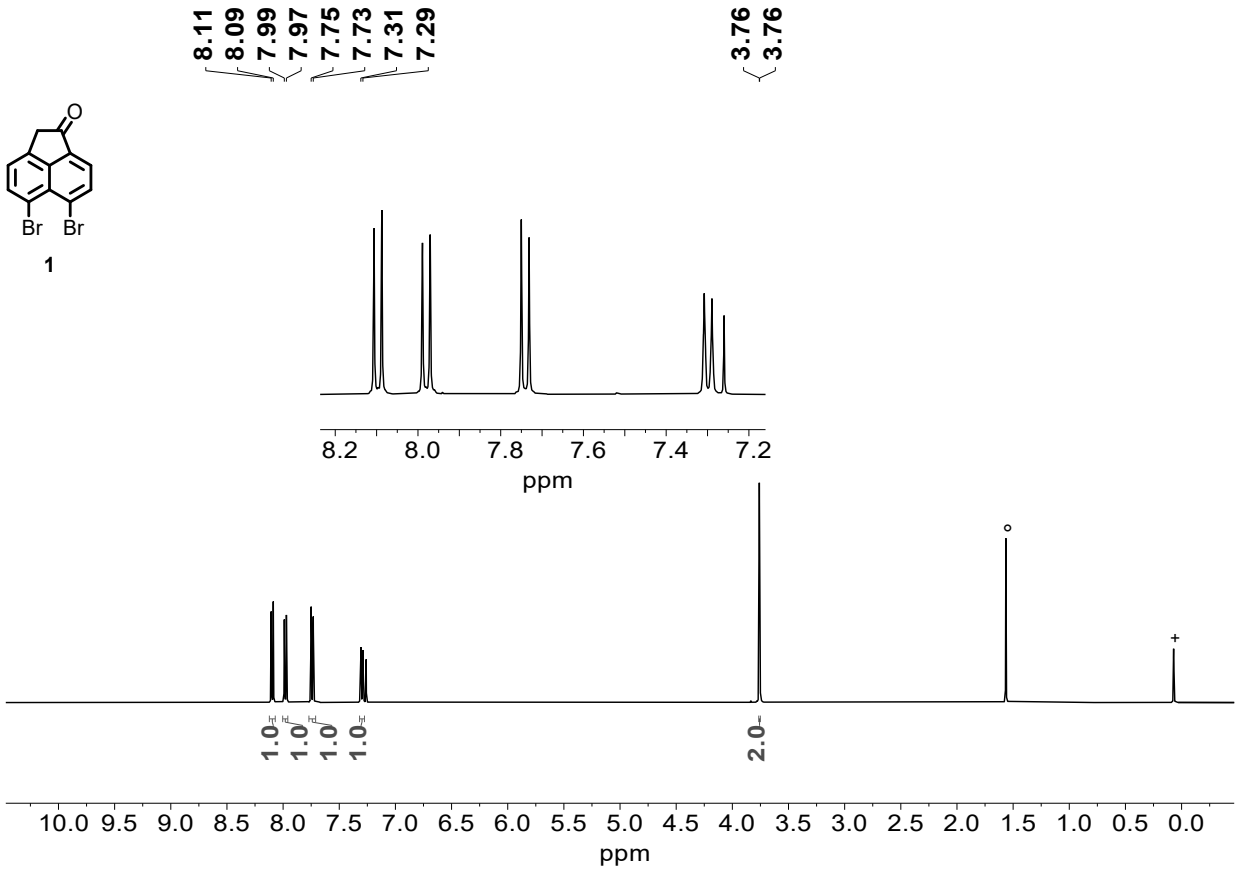

Figure S3. ^{1}H NMR spectrum of **1** (400 MHz, $CDCl_3$, rt), ° H_2O, ⁺ silicone grease.

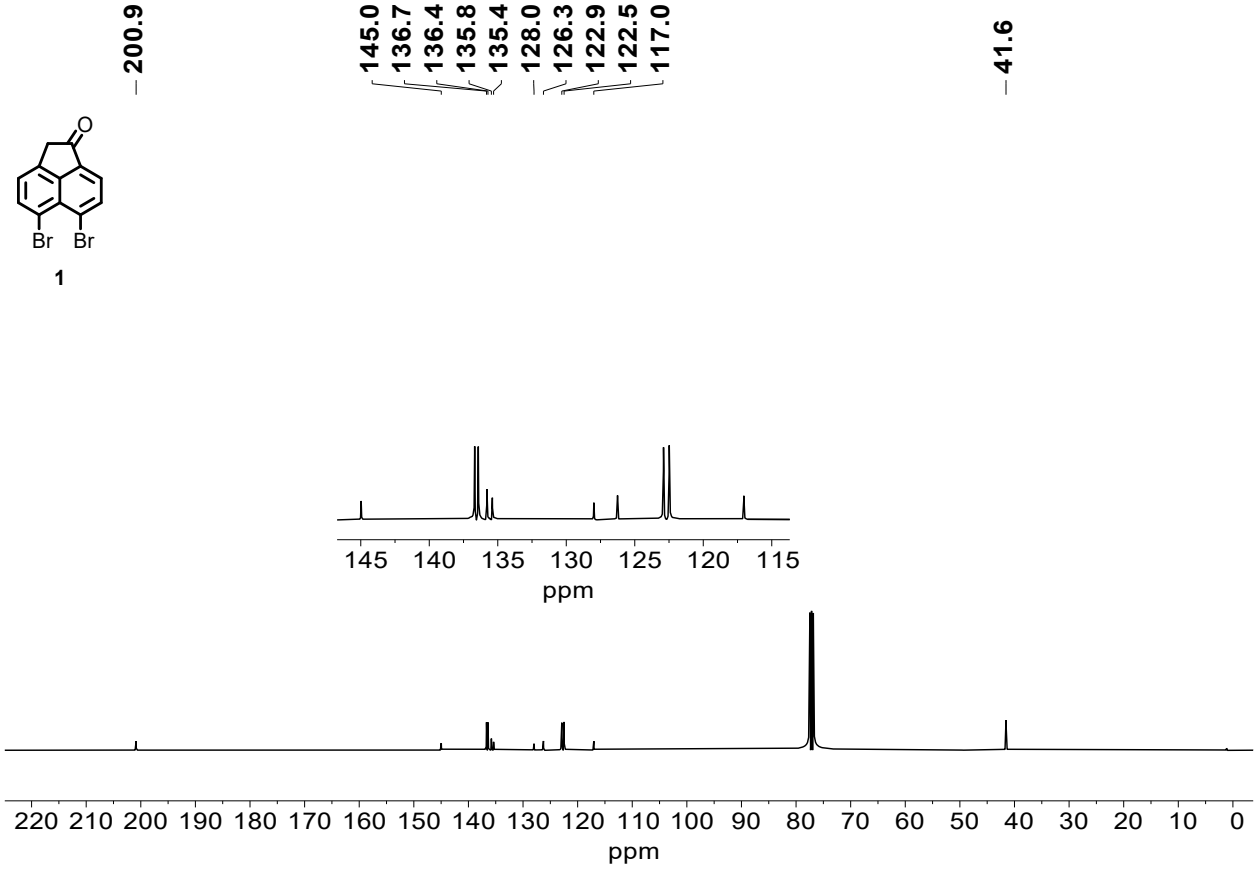

Figure S4. ^{13}C NMR spectrum of **1** (101 MHz, $CDCl_3$, rt).

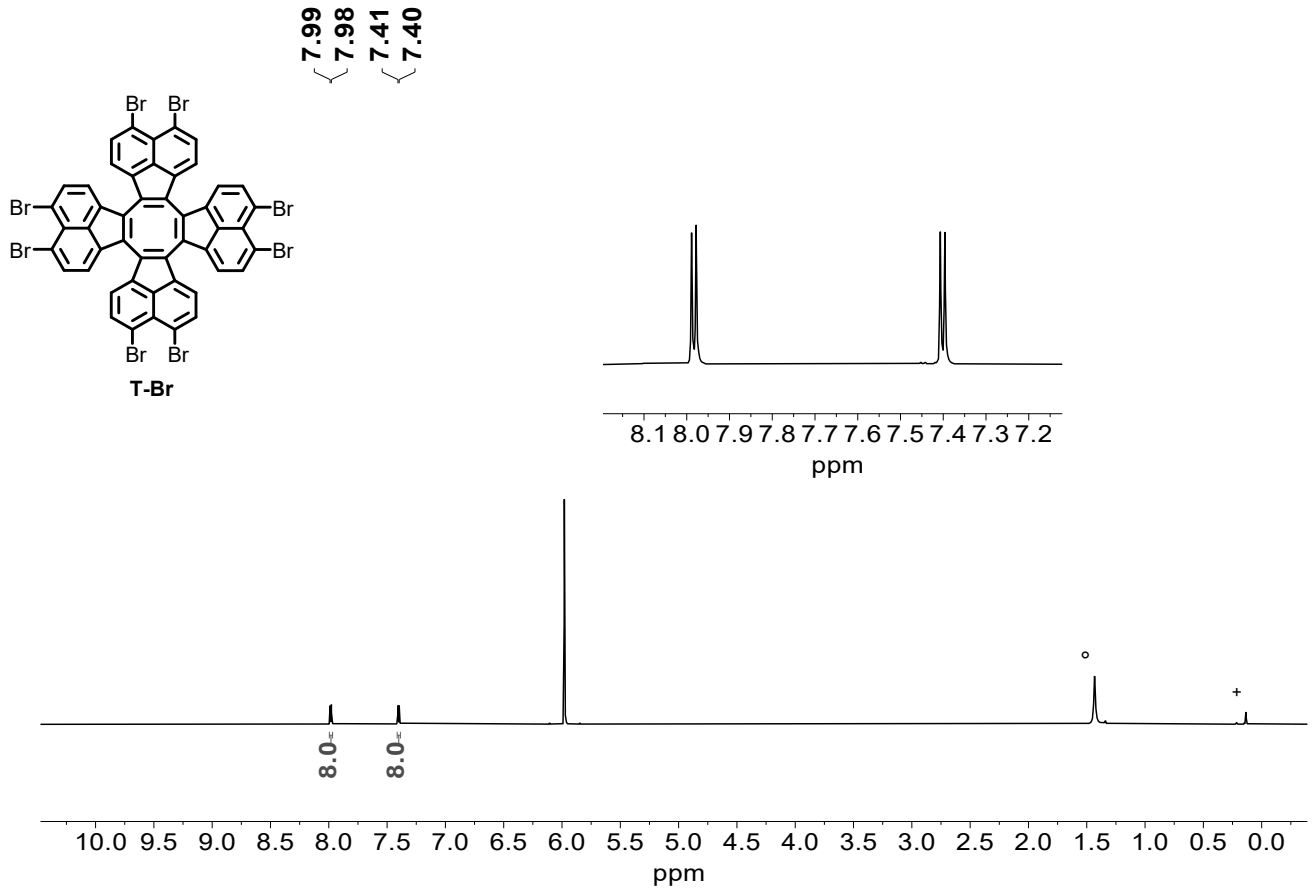

Figure S5. ^{1}H NMR spectrum of **T-Br** (700 MHz, TCE-d_2, 393 K), ° H_2O, ⁺ silicone grease.

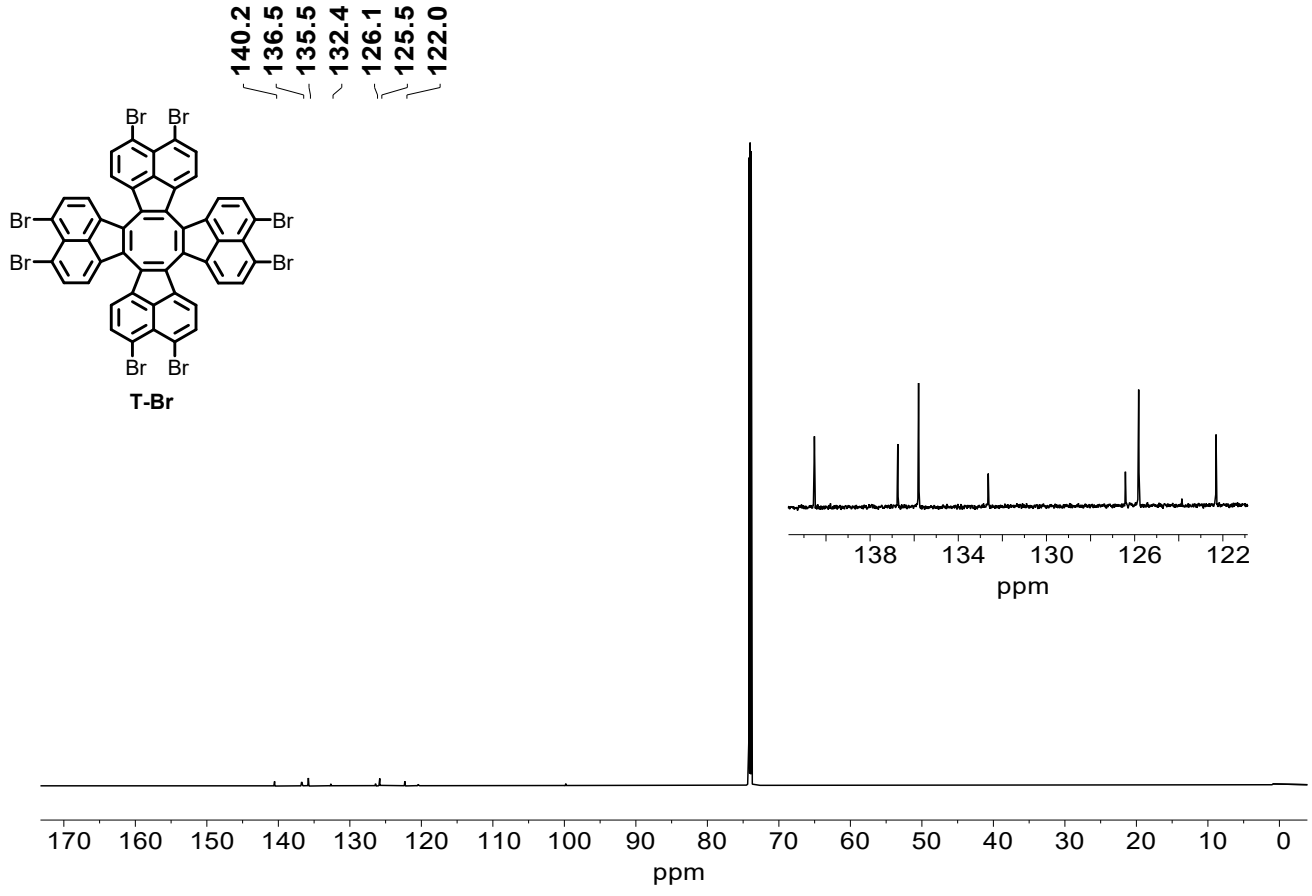

Figure S6. ^{13}C NMR spectrum of **T-Br** (176 MHz, TCE-d_2, 393 K).

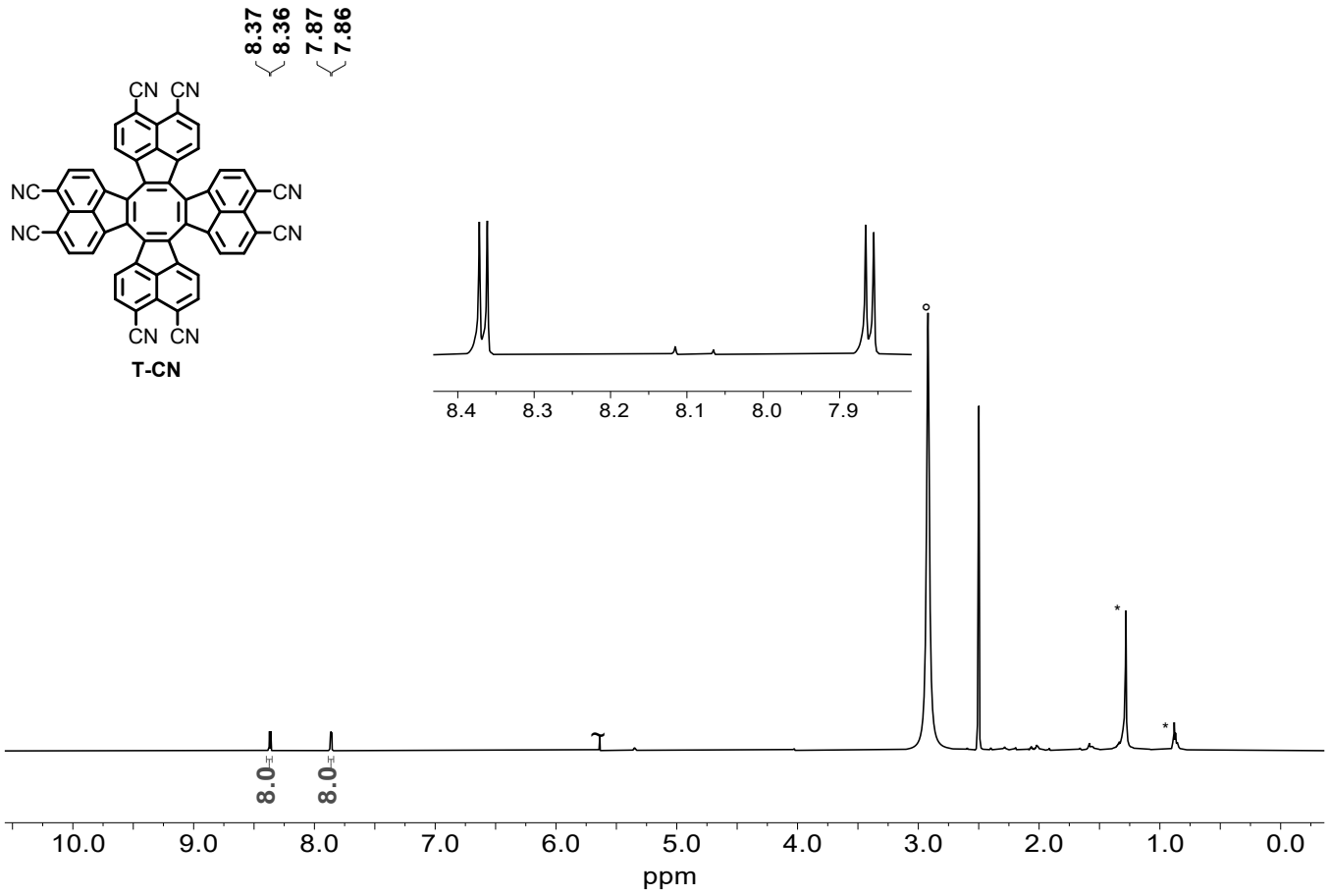

Figure S7. ^{1}H NMR spectrum of **T-CN** (700 MHz, DMSO-d_6, 393 K), °H_2O, *n-heptane, ~CH_2Cl_2.

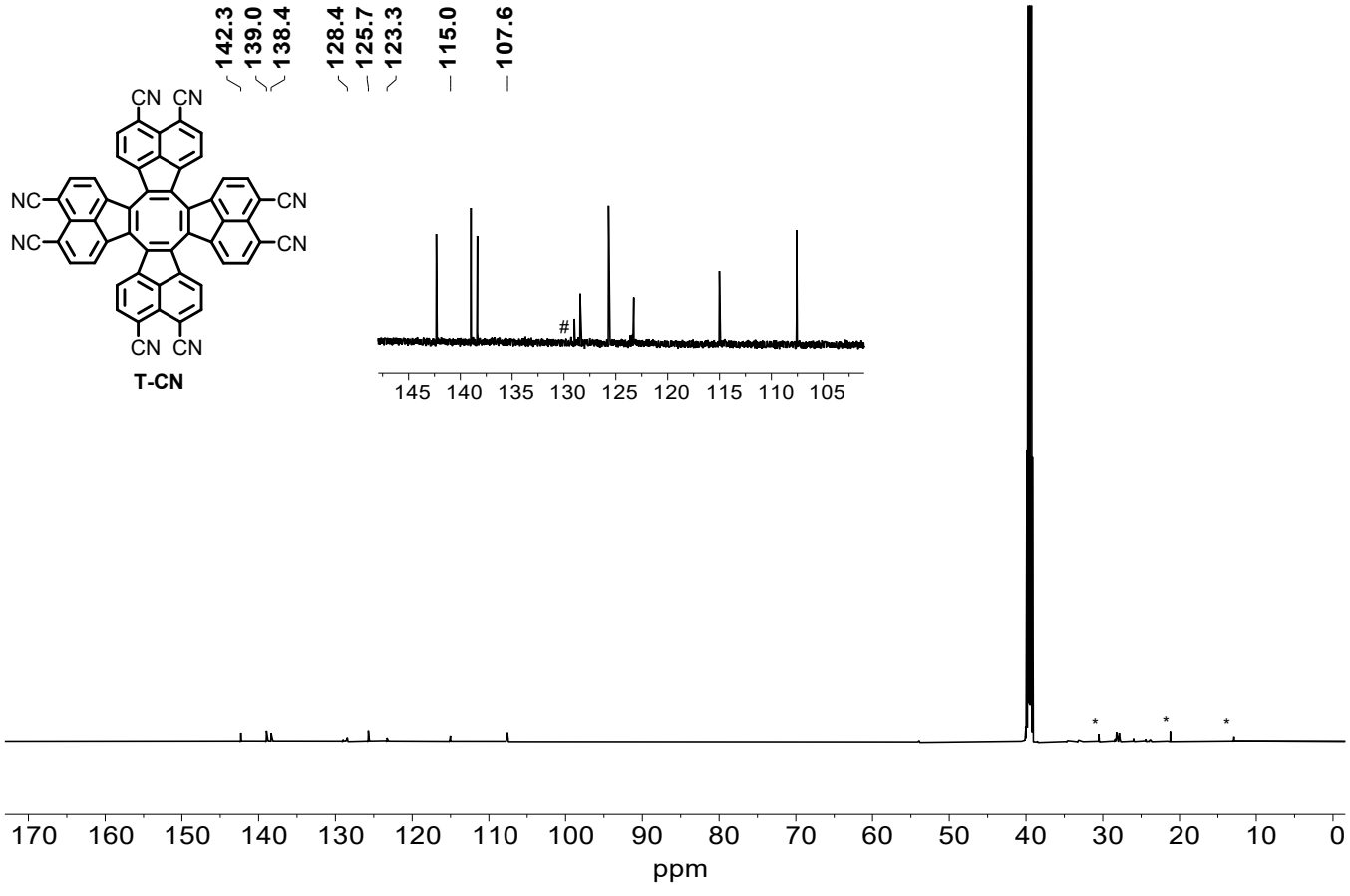

Figure S8. ^{13}C NMR spectrum of **T** (176 MHz, DMSO-d_6, 393 K), *n-heptane, # unknown aromatic impurity.

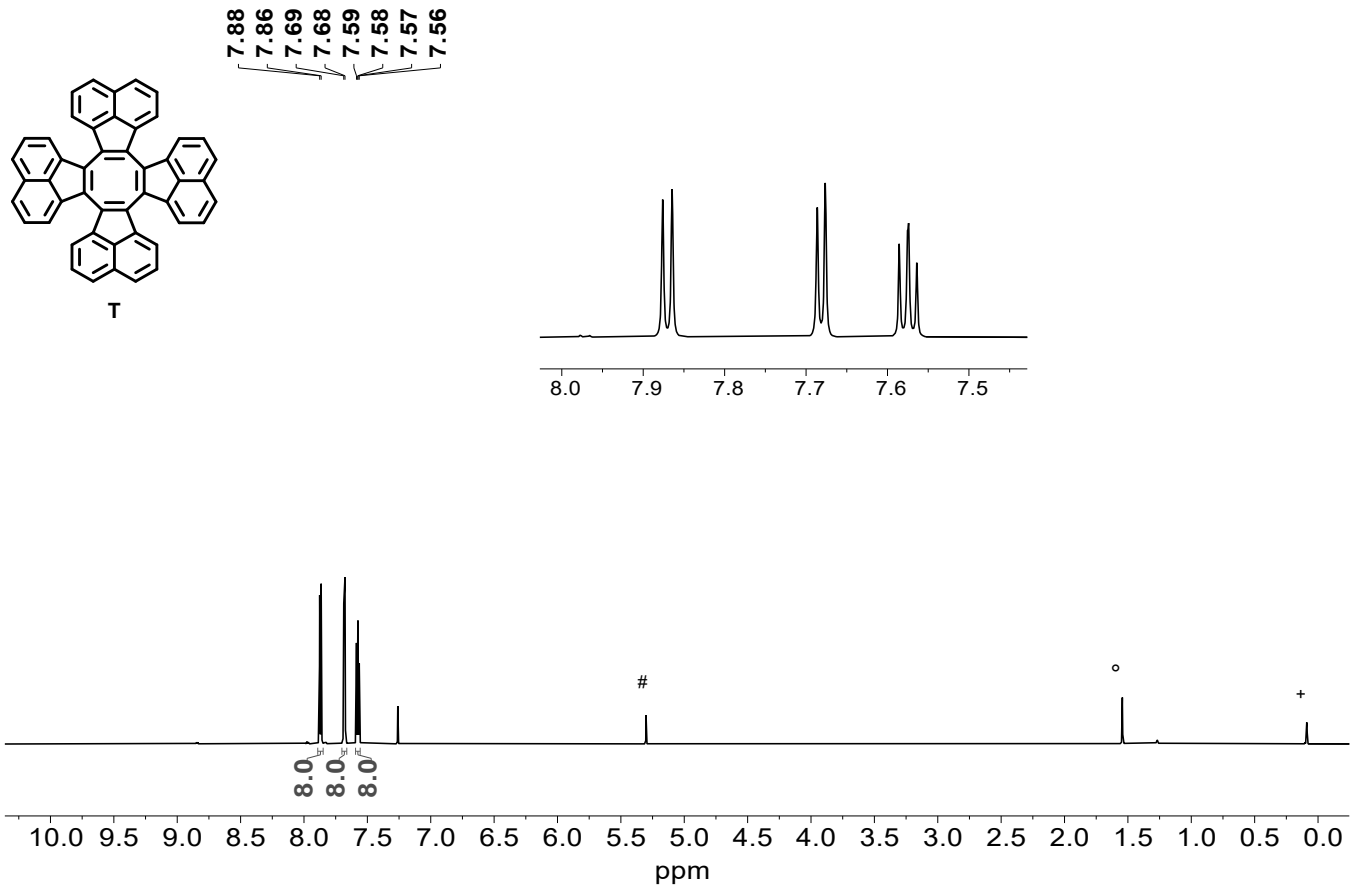

Figure S9. ^{1}H NMR spectrum of **T** (700 MHz, $CDCl_3$, rt), ° H_2O, + silicone grease, #CH_2Cl_2.

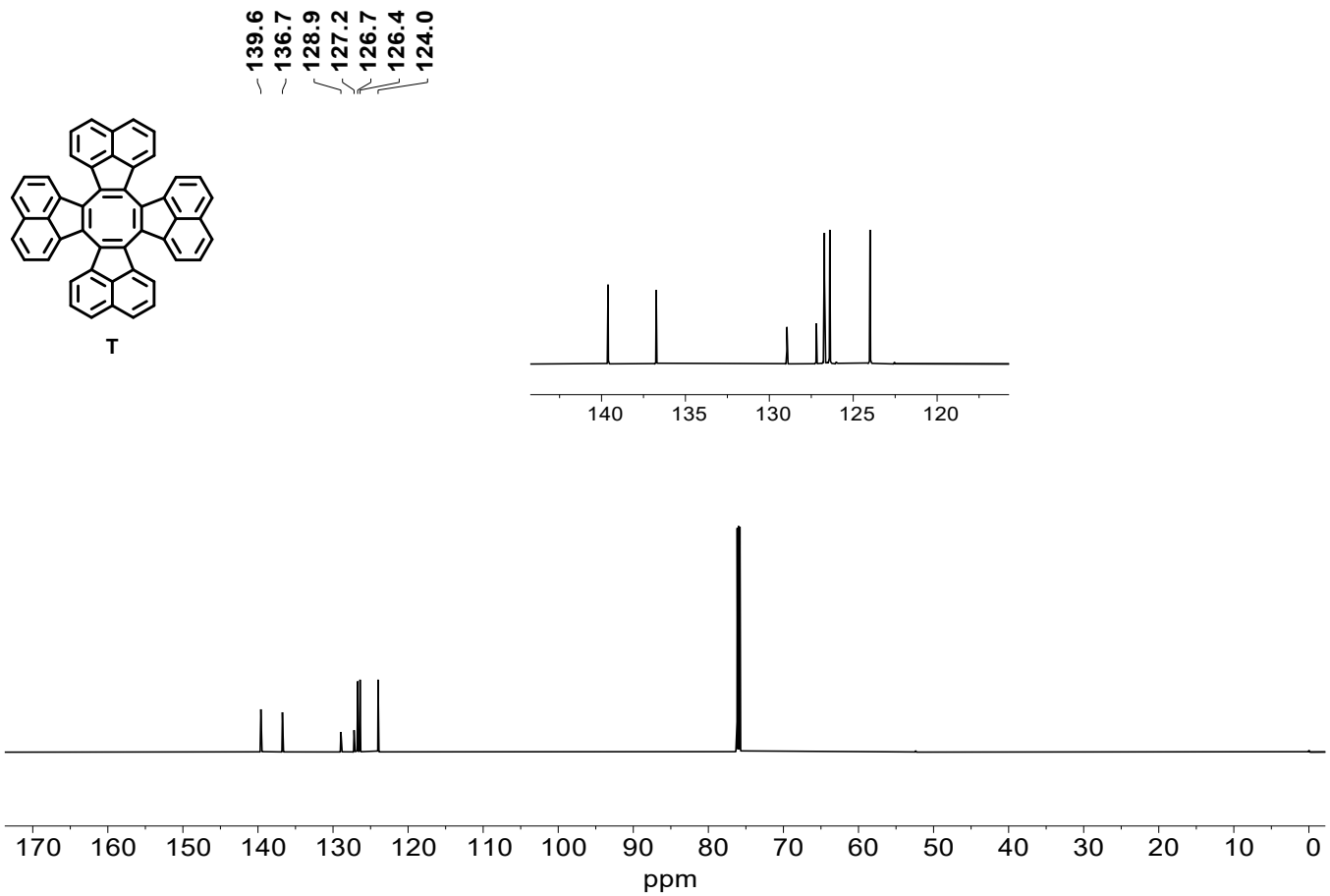

Figure S10. ^{13}C NMR spectrum of **T** (176 MHz, $CDCl_3$, rt).

3. HPLC Chromatogram of T-CN

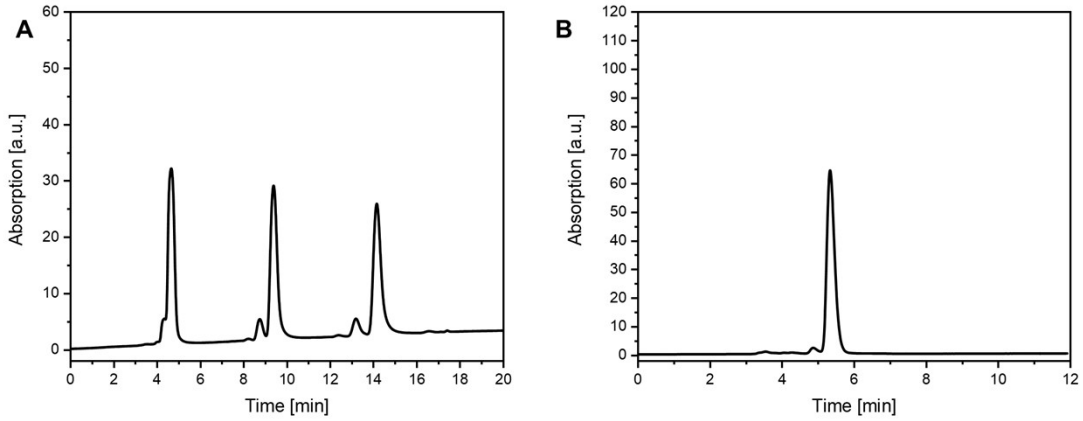

Figure S11. A. HPLC chromatogram (254 nm, CH_2Cl_2/MeOH 100:1, preparative scale) of the purification of **T-CN** after column chromatography. **B.** HPLC chromatogram (254 nm, CH_2Cl_2/MeOH 100:1, analytical scale) of the isolated fraction of **T-CN** after preparative separation.

4. X-Ray Crystallographic Data

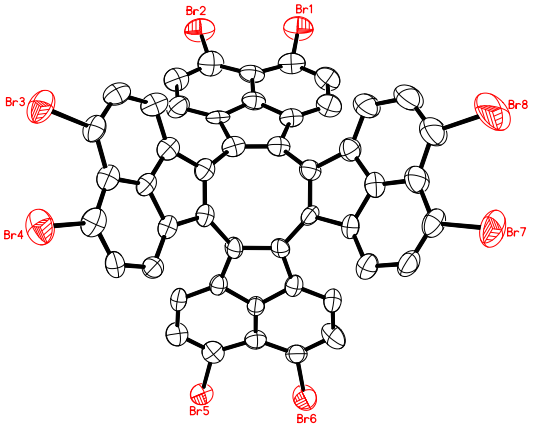

Figure S12. Crystal structure of **T-Br**. Displacement ellipsoids are displayed at 50% probability level and hydrogens are omitted for clarity. Color code: black = carbon, red = bromine.

Single crystals of **T-Br** suitable for X-ray crystallographic analysis were obtained by recrystallization from hot tetrachloroethane-d_2.

Table S1. Crystal data and structure refinement for compound **T-Br**.

CCDC	2421984	
Empirical formula	$C_{48}H_{16}Br_8$	
Formula weight	1231.89	
Temperature	200(2) K	
Wavelength	1.54178 Å	
Crystal system	triclinic	
Space group	$P\bar{1}$	
Z	4	
Unit cell dimensions	a =17.889(2) Å	α = 90.963(11) deg.
	b = 18.240(2) Å	β = 115.553(9) deg.
	c = 20.214(3) Å	γ = 101.147(10) deg.
Volume	5800.8(14) Å^3	
Density (calculated)	1.41 g cm^{-3}	
Absorption coefficient	6.81 mm^{-1}	
Crystal shape	needle	
Crystal size	0.280 x 0.014 x 0.014 mm^3	
Crystal color	brown	
Theta range for data collection	2.5 to 55.1 deg.	
Index ranges	-19≤h≤12, -19≤k≤19, -21≤l≤21	
Reflections collected	39349	
Independent reflections	14450 (R(int) = 0.0689)	
Observed reflections	9418 (I > 2σ(I))	
Absorption correction	Semi-empirical from equivalents	
Max. and min. transmission	0.90 and 0.48	
Refinement method	Full-matrix least-squares on F^2	
Data/restraints/parameters	14450 / 3572 / 1009	
Goodness-of-fit on F^2	1.05	
Final R indices (I>2sigma(I))	R1 = 0.092, wR2 = 0.204	
Largest diff. peak and hole	3.25 and -2.57 eÅ^{-3}	

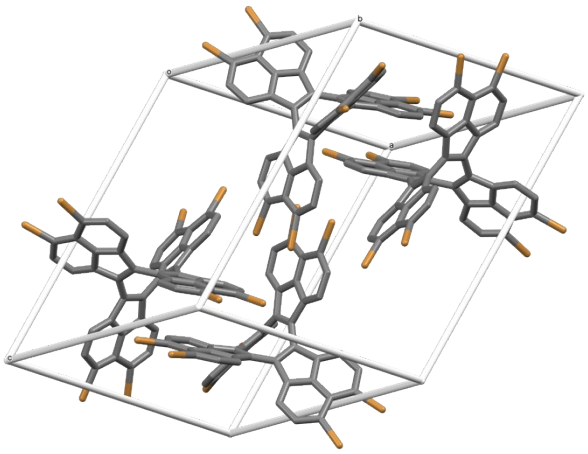

Figure S13. Unit cell of **T-Br**. H-atoms and solvent molecules omitted for clarity.

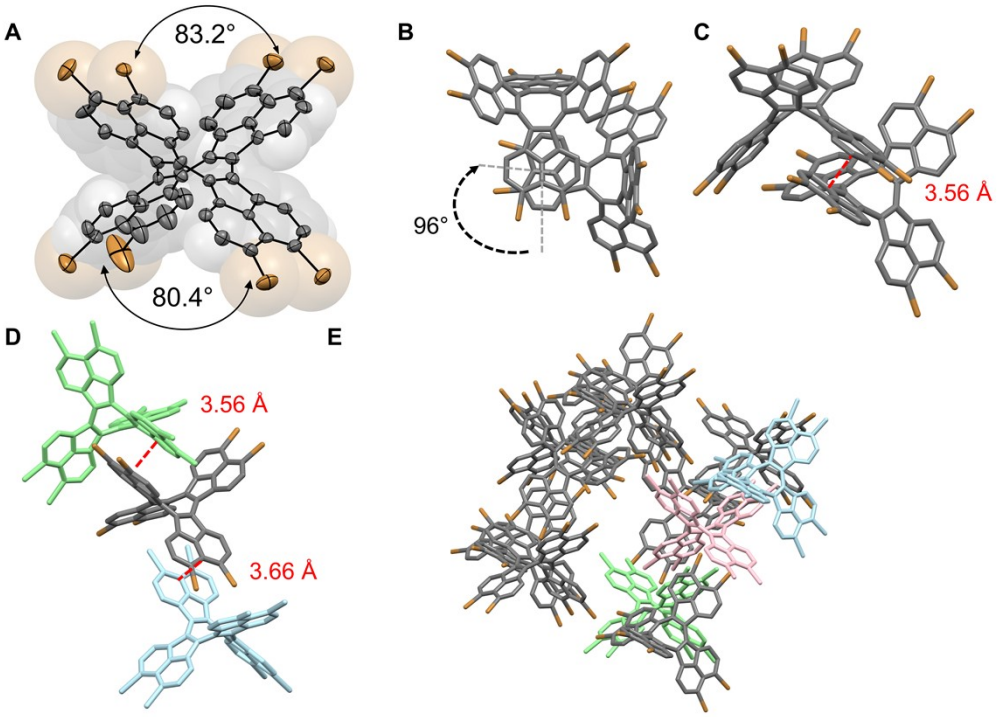

Figure S14. Molecular structure of **T-Br** obtained by single crystal X-ray diffraction. **A.** Side view on an individual molecule with highlighted splay angles. **B.** and **C.** Supramolecular motif observed in the solid state. **D.** and **E.** Packing motif with highlighted relevant short contacts. All distances are calculated upon the mean planes defined by all carbon atoms of the acenaphthylene moieties. Ellipsoids at 50% probability level, hydrogen atoms and solvent molecules omitted for clarity.

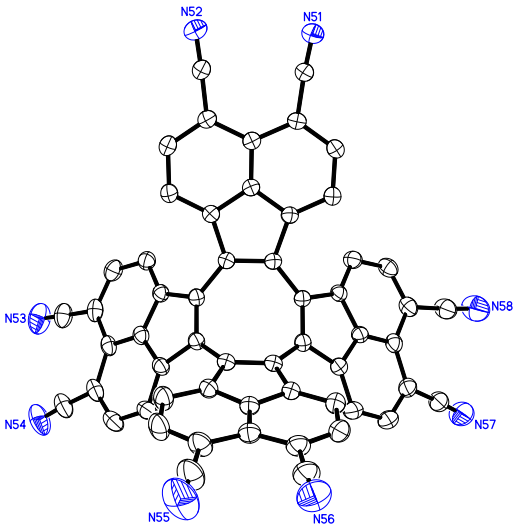

Figure S15. Crystal structure of **T-CN**. Displacement ellipsoids are displayed at 50% probability level and hydrogens are omitted for clarity. Color code: black = carbon, blue = nitrogen.

Single crystals of **T-CN** suitable for X-ray crystallographic analysis were obtained by slow evaporation of a solution of **T-CN** in nitrobenzene-d_5 at room temperature.

Table S2. Crystal data and structure refinement for compound **T-CN**.

CCDC	2421985	
Empirical formula	$C_{86}H_{41}N_{13}O_{10}$	
Formula weight	1416.32	
Temperature	200(2) K	
Wavelength	1.54178 Å	
Crystal system	triclinic	
Space group	$P\bar{1}$	
Z	2	
Unit cell dimensions	a = 14.5165(4) Å	α = 99.131(2) deg.
	b = 14.8591(5) Å	β = 96.844(2) deg.
	c = 19.1260(6) Å	γ = 118.484(2) deg.
Volume	3488.8(2) $Å^3$	
Density (calculated)	1.35 g cm^{-3}	
Absorption coefficient	0.75 mm^{-1}	
Crystal shape	prism	
Crystal size	0.095 x 0.077 x 0.070 mm^3	
Crystal color	brown	
Theta range for data collection	2.4 to 68.6 deg.	
Index ranges	-17≤h≤16, -11≤k≤17, -22≤l≤22	
Reflections collected	48296	
Independent reflections	12448 (R(int) = 0.0478)	
Observed reflections	7673 (I > 2σ(I))	
Absorption correction	Semi-empirical from equivalents	
Max. and min. transmission	0.98 and 0.84	
Refinement method	Full-matrix least-squares on F^2	
Data/restraints/parameters	12448 / 1778 / 1097	
Goodness-of-fit on F^2	0.99	
Final R indices (I>2sigma(I))	R1 = 0.052, wR2 = 0.129	
Largest diff. peak and hole	0.40 and -0.32 $eÅ^{-3}$	

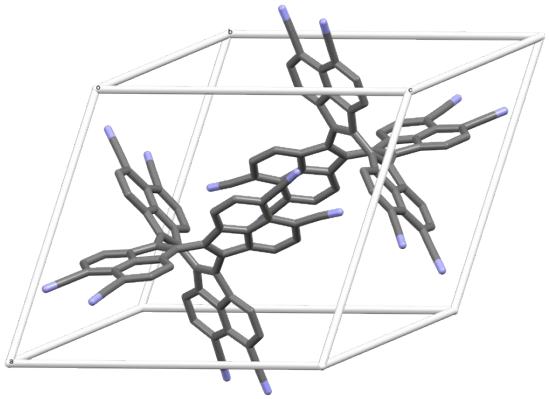

Figure S16. Unit cell of **T-CN**. H-atoms and solvent molecules omitted for clarity.

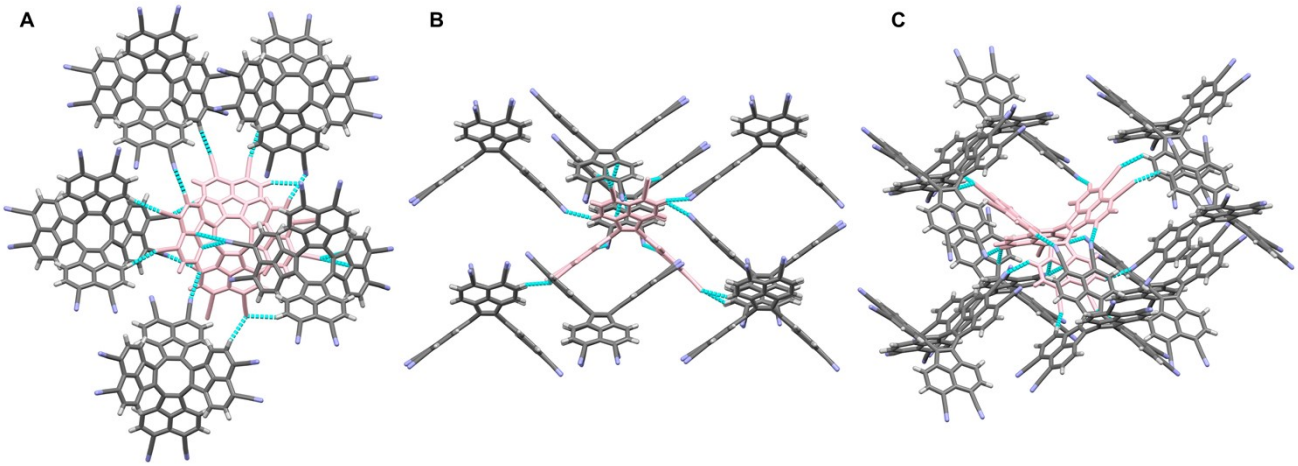

Figure S17. A., **B.** and **C.** Top, side and twisted view on a capped stick model displaying all short contact interaction (blue dotted lines) of one molecule of **T-CN** with 8 adjacent molecules. Solvent molecules omitted for clarity

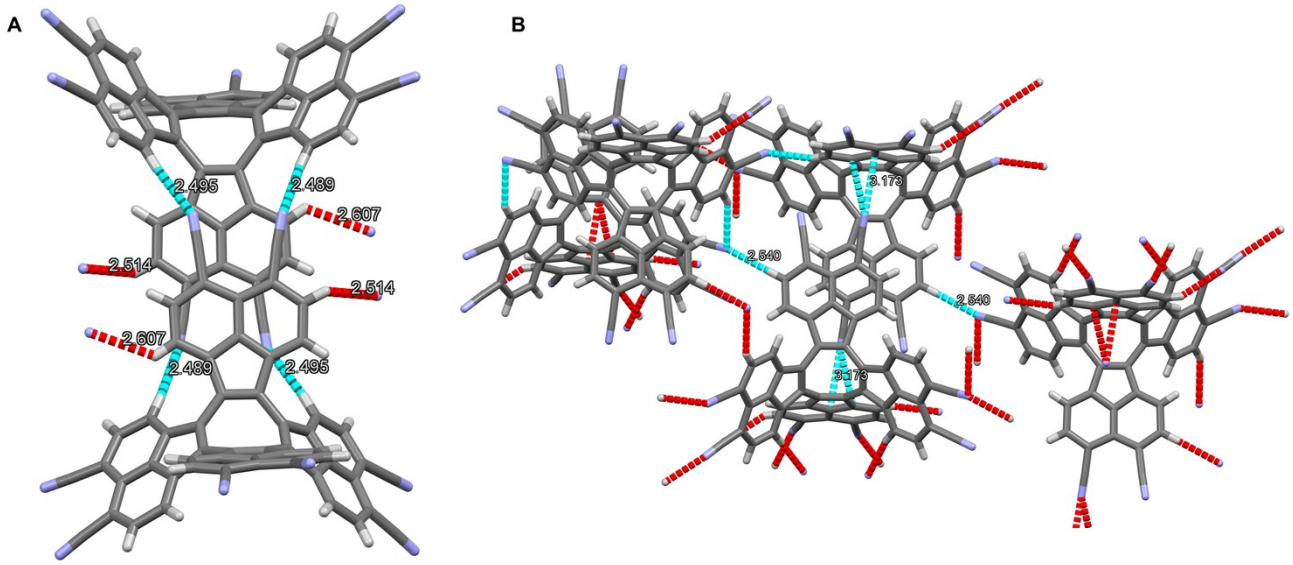

Figure S18. A. Top view on the short contact interactions between **T-CN** molecules along the crystallographic c axis. **B.** Top view on the short contact interactions between **T-CN** molecules along the crystallographic c axis on the opposing side of the molecule. Distances between atoms are reported in Ångström and were calculated using Mercury 2020.1. Solvent molecules omitted for clarity.

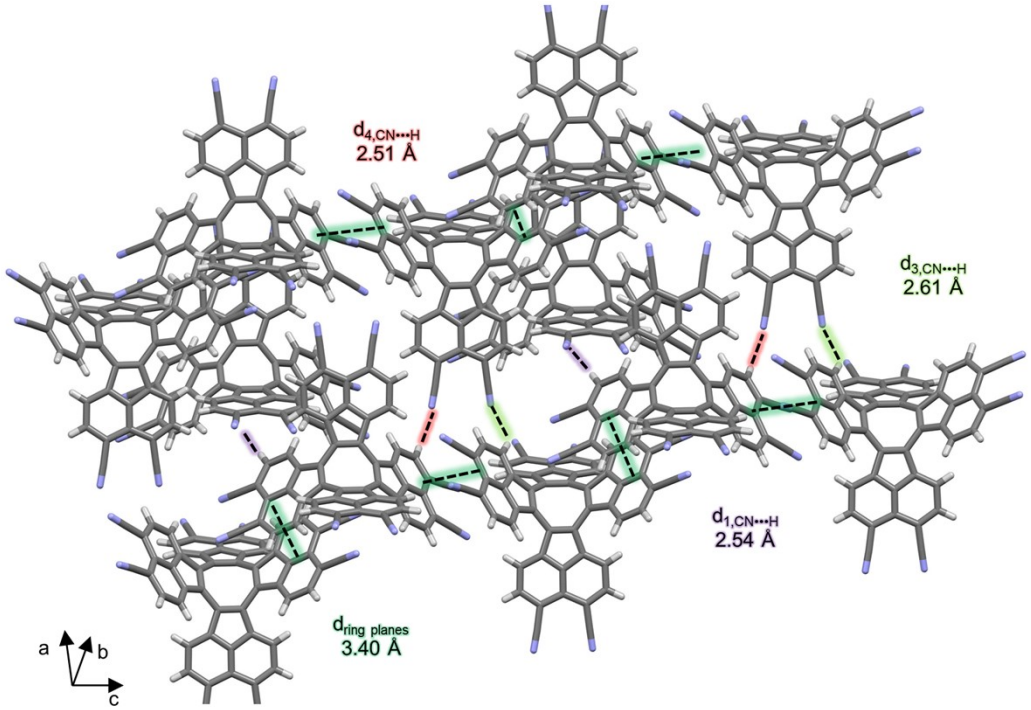

Figure S19. Solid state packing of **T-CN** highlighting the hydrogen bonding interactions along the crystallographic b axis. Solvent molecules omitted for clarity.

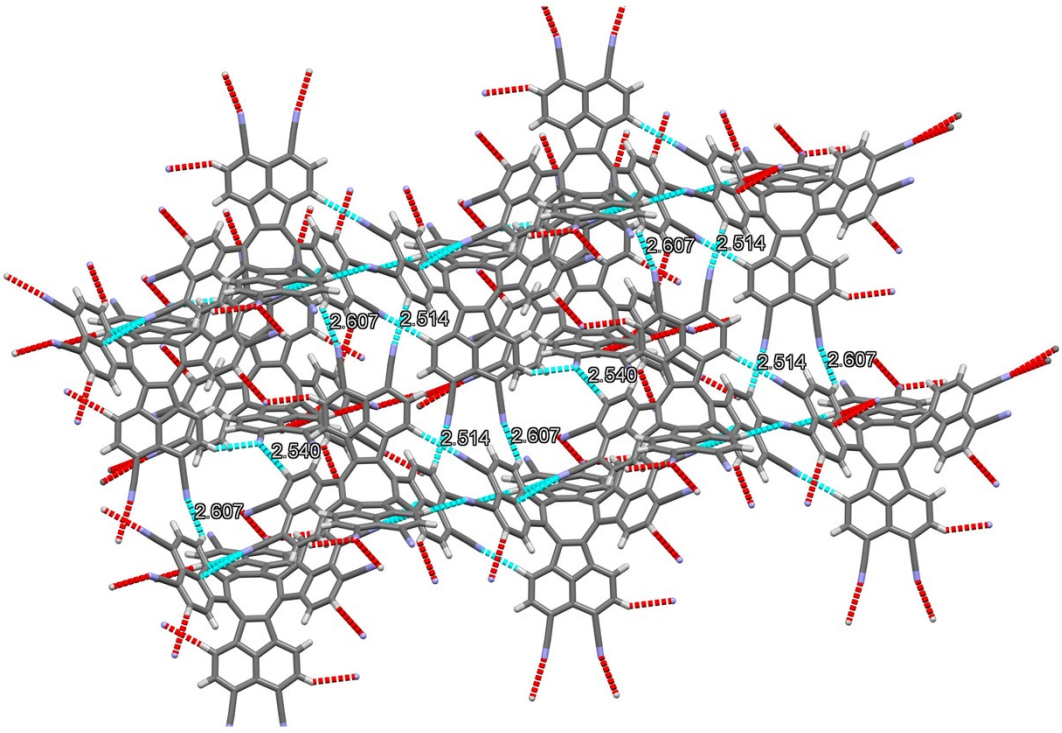

Figure S20. Solid state packing of **T-CN** showing short contact interactions. Distances between atoms are reported in Ångström and were calculated using Mercury 2020.1. Solvent molecules omitted for clarity.

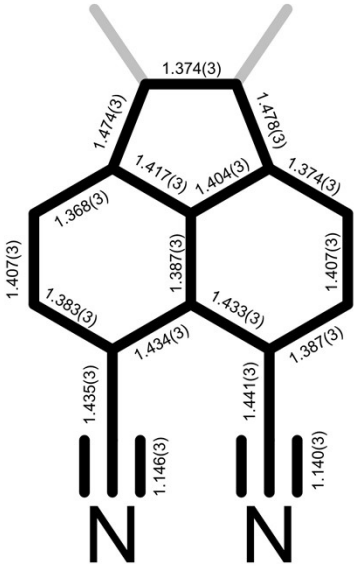

Figure S21. Representative bond lengths of one subunit of **T-CN** extracted from the typical X-ray crystal structure. Values are reported in Ångström.

5. Electrochemical Data

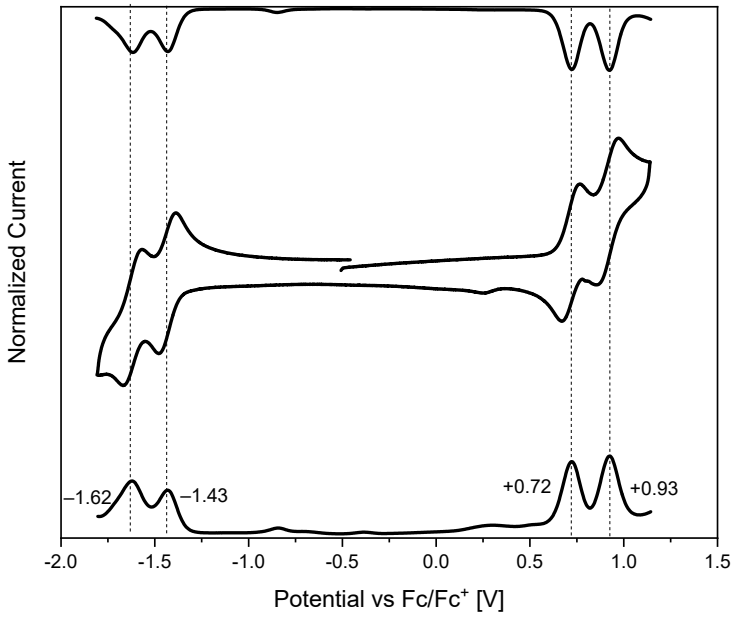

Figure S22. Differential pulse voltammogram (top), cyclic voltammogram (middle) and square wave voltammogram (bottom) of **T-Br** (*o*-DCB/MeCN (4:1) (v/v) + nBu$_4$NPF$_6$ (≈ 2mM), scan rate for cyclic voltammogram 149 mV/s, vs. Fc/Fc$^+$). Potentials extracted from square wave voltammogram.

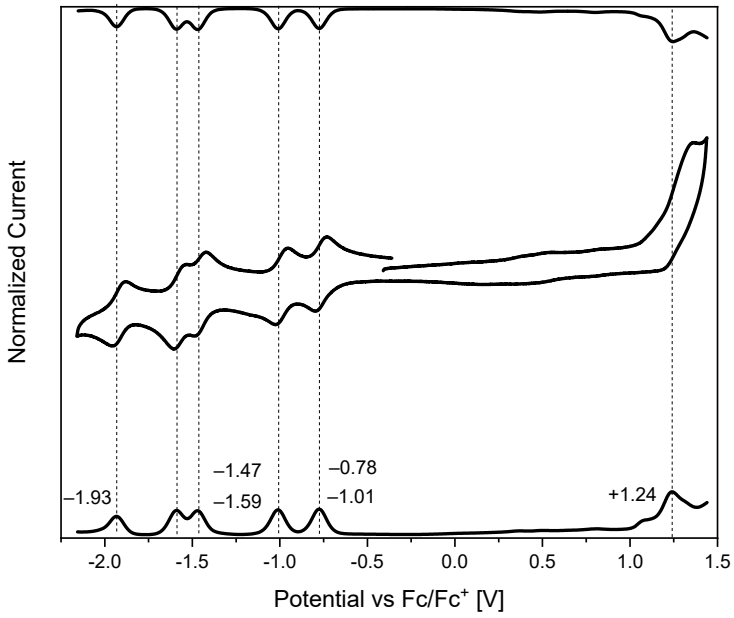

Figure S23. Differential pulse voltammogram (top), cyclic voltammogram (middle) and square wave voltammogram (bottom) of **T-CN** (CH_2Cl_2 + nBu$_4$NPF$_6$ (≈ 2mM), scan rate for cyclic voltammogram 149 mV/s, vs. Fc/Fc$^+$). Potentials extracted from square wave voltammogram.

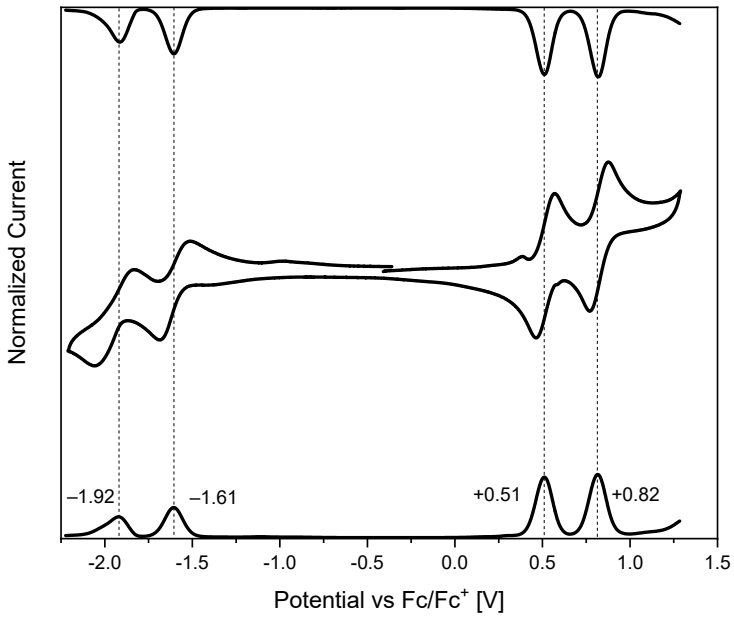

Figure S24. Differential pulse voltammogram (top), cyclic voltammogram (middle) and square wave voltammogram (bottom) of **T** (CH_2Cl_2 + nBu_4NPF_6 (≈ 2mM), scan rate for cyclic voltammogram 149 mV/s, vs. Fc/Fc^+). Potentials extracted from square wave voltammogram.

6. UV-Vis Spectroscopy Data

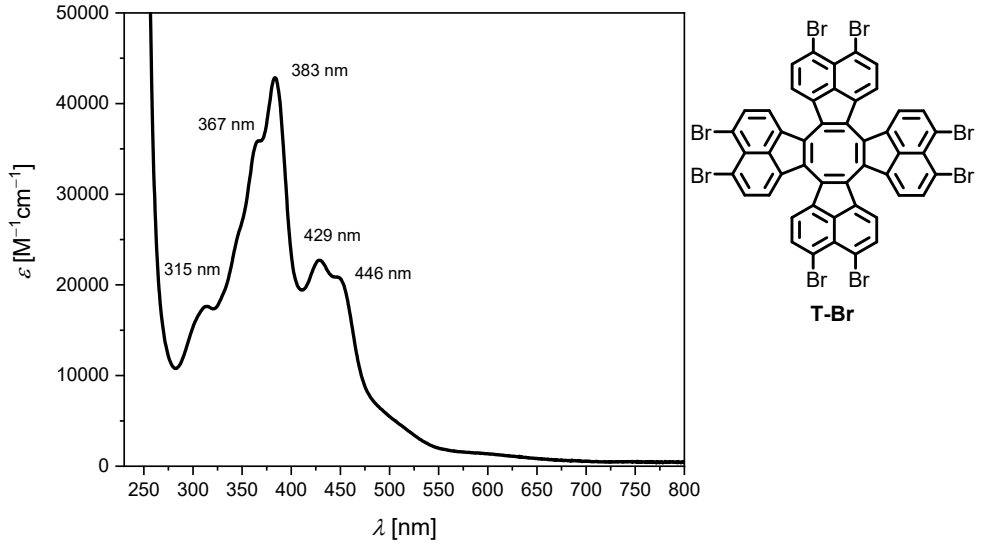

Figure S25. UV-Vis absorption spectrum of **T-Br** in CH_2Cl_2 at rt.

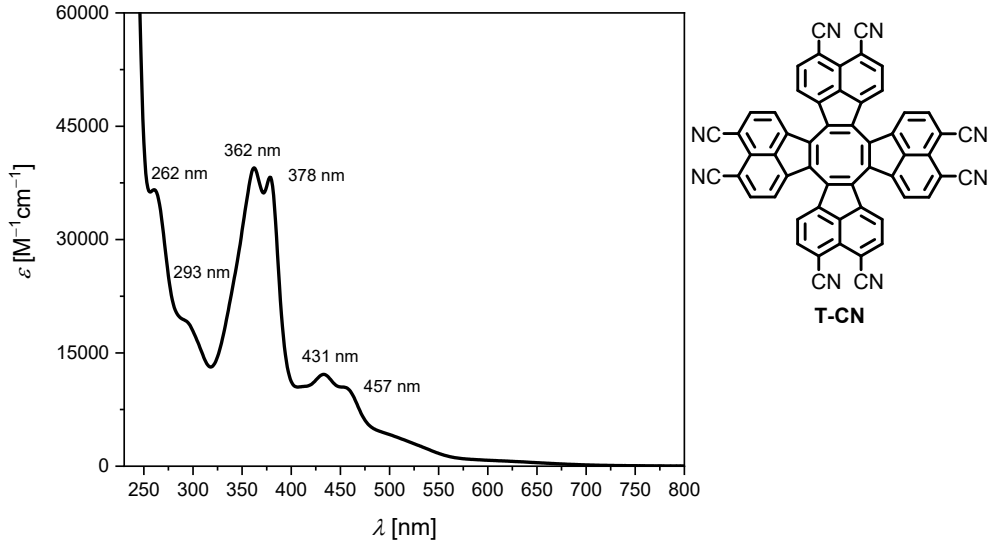

Figure S26. UV-Vis absorption spectrum of **T-CN** in CH_2Cl_2 at rt.

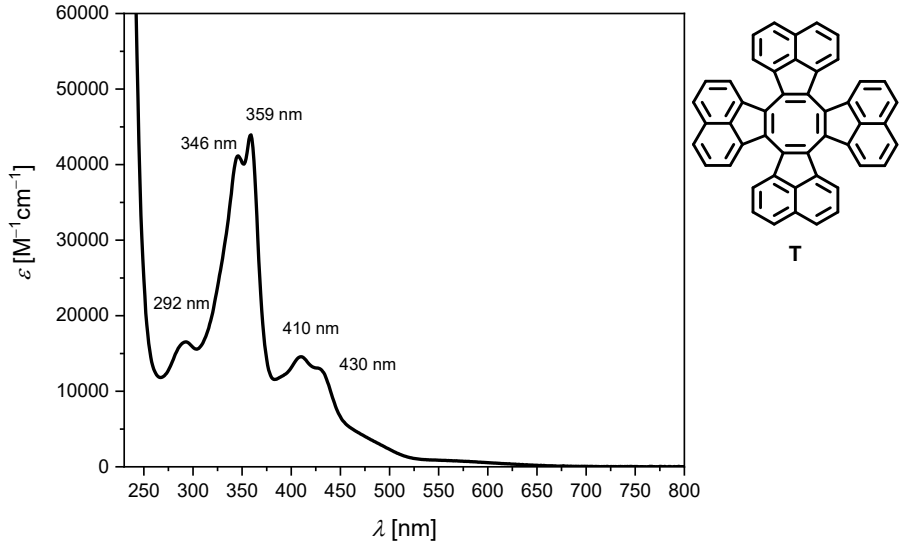

Figure S27. UV-Vis absorption spectrum of **T** in CH_2Cl_2 at rt.

7. Reduction with Sodium Metal Followed by UV-Vis-NIR Spectroscopy

Reduction of T-CN with sodium metal

All operations were performed under a nitrogen atmosphere in a glovebox using dry and degassed solvents. The reduction was performed in a sealable quartz glass cuvette (light path 10 mm), which was equipped with a magnetic stir bar. A saturated solution of **T-CN** was obtained by dissolving **T-CN** (0.2 mg, 250 nmol) in THF (2.8 mL) and filtration of the resulting suspension through a syringe filter into a cuvette equipped with a stir bar. Crown ether 18-crown-6 (0.52 mg, excess) and sodium metal (1.1 mg, excess) were added, the cuvette was sealed, exported out of the glovebox and the mixture was stirred at room temperature while the spectral changes were monitored by UV-Vis-NIR spectroscopy. After 90 min, the cuvette was imported into the glovebox, sodium metal (3.9 mg, excess) was added, the cuvette was sealed, exported out of the glovebox and the mixture was stirred at room temperature while the spectral changes were monitored by UV-Vis-NIR spectroscopy. Reoxidation was carried out by exposing the content of the cuvette to air.

After stirring the mixture in the cuvette overnight, (20 hours) a dark brown precipitate appeared, which could not be redissolved and remained unchanged after the content of the cuvette was exposed to air.

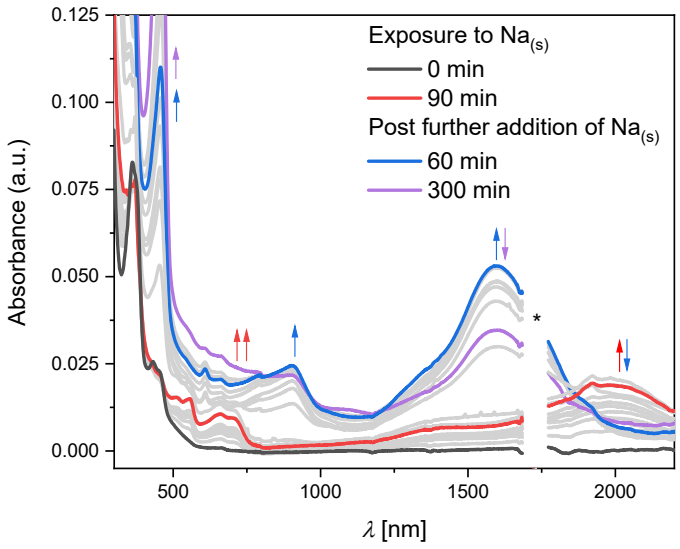

Figure S28. UV-Vis-NIR spectra recorded during the reduction of **T-CN** with sodium metal (excess) in THF in the presence of 18-crown-6 at rt (10 mm cuvette) for up to 6.5 h. * Data between 1684 and 1773 nm omitted due to solvent absorption.

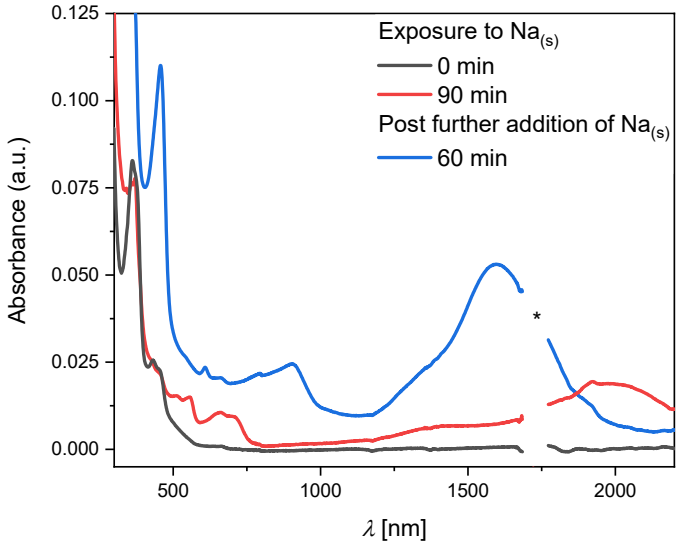

Figure S29. UV-Vis-NIR spectra recorded during the reduction of **T-CN** with sodium metal in THF in the presence of 18-crown-6 at rt (10 mm cuvette) after 0 and 90 minutes of the initially added portion of sodium metal and 60 minutes after further addition of sodium metall. * Data between 1684 and 1773 nm omitted due to solvent absorption.

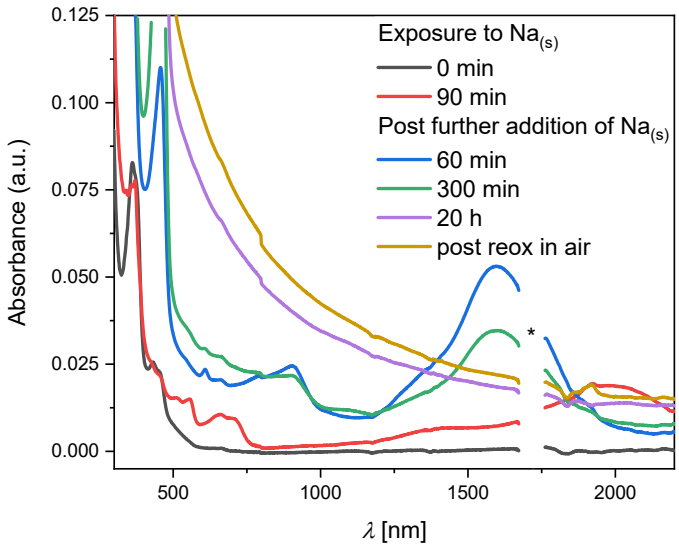

Figure S30. UV-Vis-NIR spectra of the reduction of **T-CN** with sodium metal in the presence of 18-crown-6 in THF at rt for up to 20 h and after reoxidation in air (10 mm cuvette). * Data between 1684 and 1773 nm omitted due to solvent absorption.

8. Spectroelectrochemistry

Spectroelectrochemical measurements were conducted at room temperature in 0.1 M *n*-Bu_4NPF_6 electrolyte solutions in anhydrous, degassed CH_2Cl_2. Measurements were taken across a potential range of –0.4 V to –1.5 V in 100 mV increments, with each potential held for 5 minutes before recording of the spectra. The potential is reported against an Ag microwire pseudoreference electrode.

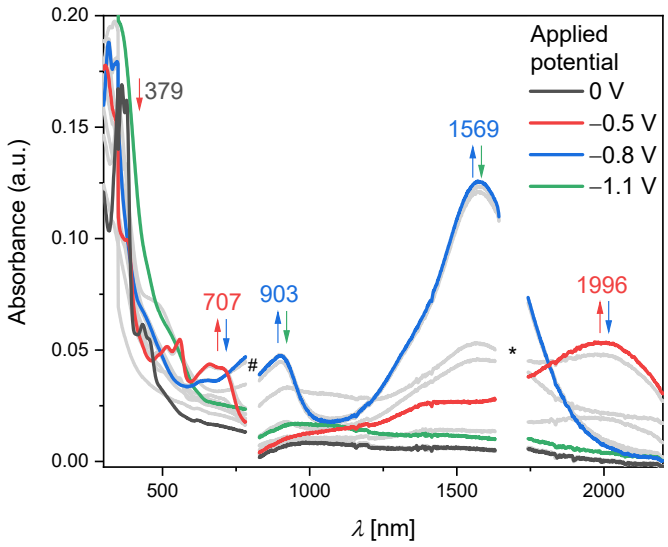

Figure S31. UV-Vis-NIR spectroelectrochemical measurement of **T-CN** in CH_2Cl_2 at rt in the potential range from –0.4 V to –1.5 V in 100 mV increments. Red, blue and green traces correspond to the maximum concentrations of **T-CN**$^{\bullet-}$, **T-CN**$^{2-}$ and an unidentified decomposition product, respectively. * Data between 1643 and 1742 nm omitted due to solvent absorption. # Data between 782 and 829 nm removed due to artifacts caused by a detector change.

9. Frontier Molecular Orbitals

In the following, selected Kohn-Sham molecular orbitals calculated at B3LYP(D3BJ)/6-311+G(d,p) in vacuum for the ground state optimized geometries are shown.

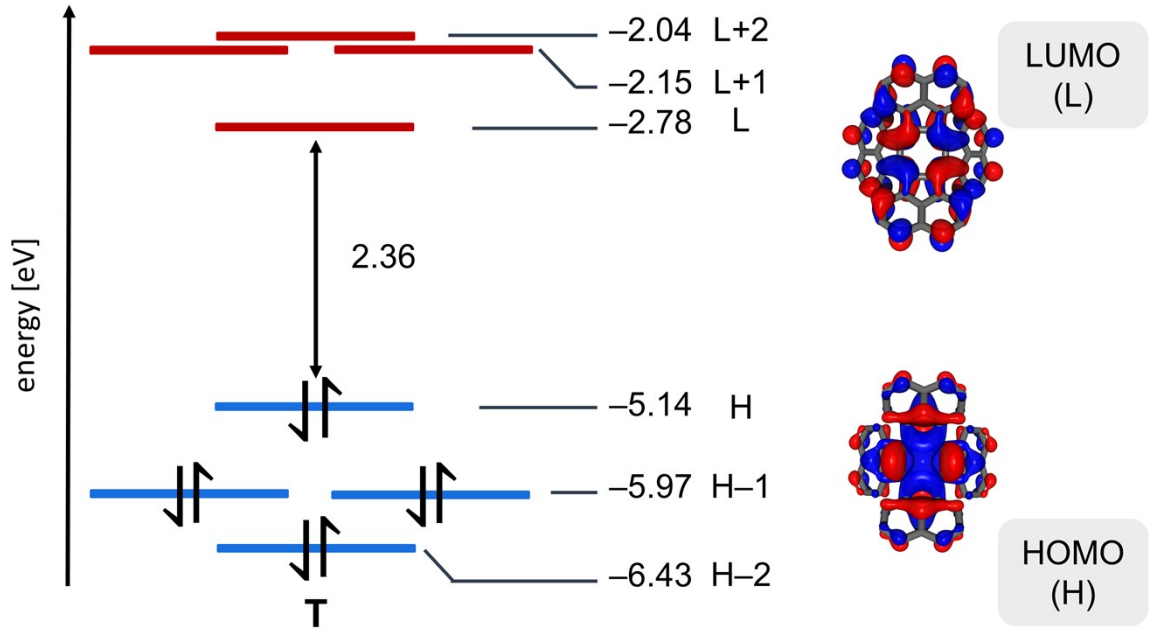

Figure S32. Frontier molecular orbitals (FMOs) of tridecacyclene **T** as calculated by DFT at the B3LYP(D3BJ)/6-311+G(d,p) level of theory. Orbital energies are given in eV. Isosurfaces plotted at 0.02 $Bohr^{-3/2}$.

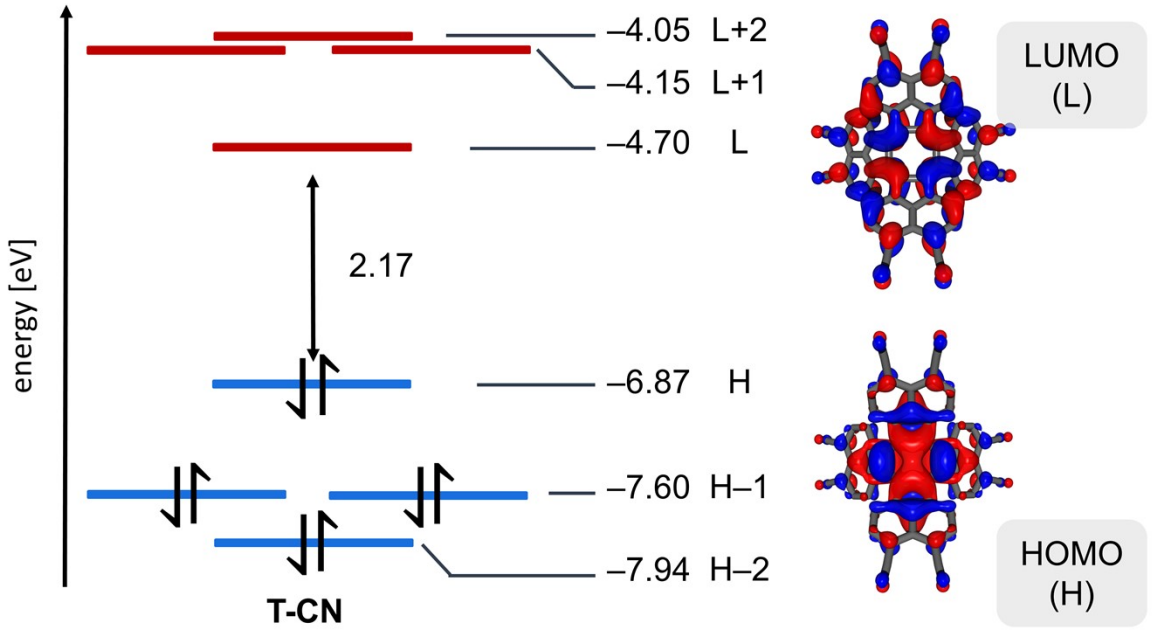

Figure S33. FMOs of octacyano-substituted tridecacyclene **T-CN** as calculated by DFT at the B3LYP(D3BJ)/6-311+G(d,p) level of theory. Orbital energies are given in eV. Isosurfaces plotted at 0.02 $Bohr^{-3/2}$.

10. DFT-Optimized Structures

Table S3. Summary of computational data for **T-CN** and its reduced states.

Charge, Multiplicity	SCF[a] Total electronic energy [Hartree]	<S²>[b]	E(HOMO)	E(LUMO)	HOMO-LUMO Gap
0, 1	-2582.359844	0	-6.87	-4.70	2.17
-1, 2	-2582.502183	0.7501	-3.05	-1.88	1.17
-2, 1	-2582.554267	0	-0.60	0.52	1.1
-2, 3	-2582.541385	2.00	-0.81	-0.26	0.55

[a] Self consistent field, [b] Expectation value of the total spin after annihilation of the first spin contamination

Table S4. Atom coordinates of optimized structure of **T-CN** (charge 0, multiplicity 1).

atom	x	y	z
C	-1.26509	1.16053	0.37366
C	-0.00392	1.71678	0.37366
C	-2.14088	1.98841	1.22648
C	-3.454	1.90786	1.63581
C	-3.94642	2.90155	2.51279
C	-3.15976	3.94642	2.99373
C	-0.02469	2.92168	1.22654
C	-1.34435	3.04812	1.7229
C	-1.78107	4.03837	2.6018
C	-0.78348	4.99443	2.99376
C	0.51855	4.8707	2.51282
C	0.92028	3.837	1.63586
C	3.454	-1.90786	1.63581
C	3.94642	-2.90155	2.51279
C	3.15976	-3.94642	2.99373
C	1.78107	-4.03837	2.6018
C	1.34435	-3.04812	1.7229
C	2.14088	-1.98841	1.22648
C	0.78348	-4.99443	2.99376
C	-0.51855	-4.8707	2.51282
C	-0.92028	-3.837	1.63586
C	0.02469	-2.92168	1.22654
C	1.26509	-1.16053	0.37366
C	0.00392	-1.71678	0.37366
C	1.90786	3.454	-1.63581
C	2.90155	3.94642	-2.51279
C	3.94642	3.15976	-2.99373
C	4.03837	1.78107	-2.6018
C	3.04812	1.34435	-1.7229
C	1.98841	2.14088	-1.22648
C	4.99443	0.78348	-2.99376
C	4.8707	-0.51855	-2.51282
C	3.837	-0.92028	-1.63586
C	2.92168	0.02469	-1.22654
C	1.16053	1.26509	-0.37366
C	1.71678	0.00392	-0.37366
C	-1.16053	-1.26509	-0.37366
C	-1.71678	-0.00392	-0.37366
C	-1.98841	-2.14088	-1.22648
C	-1.90786	-3.454	-1.63581
C	-2.90155	-3.94642	-2.51279
C	-3.94642	-3.15976	-2.99373
C	-2.92168	-0.02469	-1.22654
C	-3.04812	-1.34435	-1.7229
C	-4.03837	-1.78107	-2.6018
C	-4.99443	-0.78348	-2.99376
C	-4.8707	0.51855	-2.51282
C	-3.837	0.92028	-1.63586
C	-1.05468	6.08546	3.87294
N	-1.20382	6.99019	4.57512
C	-6.08546	-1.05468	-3.87294
N	-6.99019	-1.20382	-4.57512
C	6.08546	1.05468	-3.87294
N	6.99019	1.20382	-4.57512
C	1.05468	-6.08546	3.87294
N	1.20382	-6.99019	4.57512
C	-4.88248	-3.78253	-3.87284
N	-5.60274	-4.35006	-4.57496
C	3.78253	-4.88248	3.87284

N	4.35006	-5.60274	4.57496
C	4.88248	3.78253	-3.87284
N	5.60274	4.35006	-4.57496
C	-3.78253	4.88248	3.87284
N	-4.35006	5.60274	4.57496
H	-4.11077	1.10964	1.31345
H	-4.97863	2.85315	2.83549
H	1.25037	5.60026	2.83552
H	1.9526	3.78365	1.31355
H	4.11077	-1.10964	1.31345
H	4.97863	-2.85315	2.83549
H	-1.25037	-5.60026	2.83552
H	-1.9526	-3.78365	1.31355
H	1.10964	4.11077	-1.31345
H	2.85315	4.97863	-2.83549
H	5.60026	-1.25037	-2.83552
H	3.78365	-1.9526	-1.31355
H	-1.10964	-4.11077	-1.31345
H	-2.85315	-4.97863	-2.83549
H	-5.60026	1.25037	-2.83552
H	-3.78365	1.9526	-1.31355

Table S5. Atom coordinates of optimized structure of **T-CN**$^{\bullet-}$ (charge –1, multiplicity 2).

atom	x	y	z
C	0.01063	1.73982	0.34543
C	1.28555	1.17216	0.34584
C	0.05778	2.97294	1.14693
C	-0.88167	3.90122	1.55881
C	-0.46384	4.95852	2.38972
C	0.85079	5.10377	2.84069
C	2.1699	2.03233	1.14782
C	1.38732	3.11715	1.61813
C	1.84007	4.13452	2.46045
C	3.22193	4.04751	2.84202
C	3.99368	2.97294	2.39209
C	3.48794	1.95496	1.56091
C	0.88167	-3.90122	1.55881
C	0.46384	-4.95852	2.38972
C	-0.85079	-5.10377	2.84069
C	-1.84007	-4.13452	2.46045
C	-1.38732	-3.11715	1.61813
C	-0.05778	-2.97294	1.14693
C	-3.22193	-4.04751	2.84202
C	-3.99368	-2.97294	2.39209
C	-3.48794	-1.95496	1.56091
C	-2.1699	-2.03233	1.14782
C	-0.01063	-1.73982	0.34543
C	-1.28555	-1.17216	0.34584
C	3.90122	0.88167	-1.55881
C	4.95852	0.46384	-2.38972
C	5.10377	-0.85079	-2.84069
C	4.13452	-1.84007	-2.46045
C	3.11715	-1.38732	-1.61813
C	2.97294	-0.05778	-1.14693
C	4.04751	-3.22193	-2.84202
C	2.97294	-3.99368	-2.39209
C	1.95496	-3.48794	-1.56091
C	2.03233	-2.1699	-1.14782
C	1.73982	-0.01063	-0.34543
C	1.17216	-1.28555	-0.34584
C	-1.73982	0.01063	-0.34543
C	-1.17216	1.28555	-0.34584
C	-2.97294	0.05778	-1.14693
C	-3.90122	-0.88167	-1.55881
C	-4.95852	-0.46384	-2.38972
C	-5.10377	0.85079	-2.84069
C	-2.03233	2.1699	-1.14782
C	-3.11715	1.38732	-1.61813
C	-4.13452	1.84007	-2.46045
C	-4.04751	3.22193	-2.84202
C	-2.97294	3.99368	-2.39209
C	-1.95496	3.48794	-1.56091
C	3.86621	5.0037	3.68014
N	4.45786	5.73811	4.34929
C	-5.0037	3.86621	-3.68014
N	-5.73811	4.45786	-4.34929
C	5.0037	-3.86621	-3.68014
N	5.73811	-4.45786	-4.34929
C	-3.86621	-5.0037	3.68014
N	-4.45786	-5.73811	4.34929
C	-6.22279	1.12998	-3.67839
N	-7.15427	1.27964	-4.34706
C	-1.12998	-6.22279	3.67839
N	-1.27964	-7.15427	4.34706
C	6.22279	-1.12998	-3.67839
N	7.15427	-1.27964	-4.34706

C	1.12998	6.22279	3.67839
N	1.27964	7.15427	4.34706
H	-1.92127	3.83253	1.26574
H	-1.19094	5.69562	2.7075
H	5.02764	2.92548	2.71091
H	4.13244	1.13607	1.26869
H	1.92127	-3.83253	1.26574
H	1.19094	-5.69562	2.7075
H	-5.02764	-2.92548	2.71091
H	-4.13244	-1.13607	1.26869
H	3.83253	1.92127	-1.26574
H	5.69562	1.19094	-2.7075
H	2.92548	-5.02764	-2.71091
H	1.13607	-4.13244	-1.26869
H	-3.83253	-1.92127	-1.26574
H	-5.69562	-1.19094	-2.7075
H	-2.92548	5.02764	-2.71091
H	-1.13607	4.13244	-1.26869

Table S6. Atom coordinates of optimized structure of **T-CN**$^{2-}$ (charge –2, multiplicity 1).

atom	x	y	z
C	-0.70612	1.60909	0.32608
C	0.70612	1.60909	0.32608
C	-1.15602	2.77351	1.09531
C	-2.39422	3.24728	1.51235
C	-2.44122	4.39603	2.31419
C	-1.29772	5.08388	2.74703
C	1.15602	2.77351	1.09532
C	0	3.46069	1.55279
C	0	4.594	2.37268
C	1.29772	5.08387	2.74704
C	2.44122	4.39603	2.31421
C	2.39422	3.24728	1.51236
C	2.39422	-3.24728	1.51235
C	2.44122	-4.39603	2.31419
C	1.29772	-5.08388	2.74703
C	0	-4.594	2.37268
C	0	-3.46069	1.55279
C	1.15602	-2.77351	1.09531
C	-1.29772	-5.08387	2.74704
C	-2.44122	-4.39603	2.31421
C	-2.39422	-3.24728	1.51236
C	-1.15602	-2.77351	1.09532
C	0.70612	-1.60909	0.32608
C	-0.70612	-1.60909	0.32608
C	3.24728	2.39422	-1.51235
C	4.39603	2.44122	-2.31419
C	5.08388	1.29772	-2.74703
C	4.594	0	-2.37268
C	3.46069	0	-1.55279
C	2.77351	1.15602	-1.09531
C	5.08387	-1.29772	-2.74704
C	4.39603	-2.44122	-2.31421
C	3.24728	-2.39422	-1.51236
C	2.77351	-1.15602	-1.09532
C	1.60909	0.70612	-0.32608
C	1.60909	-0.70612	-0.32608
C	-1.60909	-0.70612	-0.32608
C	-1.60909	0.70612	-0.32608
C	-2.77351	-1.15602	-1.09531
C	-3.24728	-2.39422	-1.51235
C	-4.39603	-2.44122	-2.31419
C	-5.08388	-1.29772	-2.74703
C	-2.77351	1.15602	-1.09532
C	-3.46069	0	-1.55279
C	-4.594	0	-2.37268
C	-5.08387	1.29772	-2.74704
C	-4.39603	2.44122	-2.31421
C	-3.24728	2.39422	-1.51236
C	1.50641	6.2329	3.55928
N	1.76334	7.15745	4.20835
C	-6.2329	1.50641	-3.55928
N	-7.15745	1.76334	-4.20835
C	6.2329	-1.50641	-3.55928
N	7.15745	-1.76334	-4.20835
C	-1.50641	-6.2329	3.55928
N	-1.76334	-7.15745	4.20835
C	-6.23291	-1.50642	-3.55927
N	-7.15746	-1.76334	-4.20834
C	1.50642	-6.23291	3.55927
N	1.76334	-7.15746	4.20834
C	6.23291	1.50642	-3.55927
N	7.15746	1.76334	-4.20834
C	-1.50642	6.23291	3.55927
N	-1.76334	7.15746	4.20834
H	-3.31499	2.75046	1.23661

H	-3.40544	4.77598	2.63094
H	3.40544	4.77597	2.63096
H	3.31499	2.75045	1.23662
H	3.31499	-2.75046	1.23661
H	3.40544	-4.77598	2.63094
H	-3.40544	-4.77597	2.63096
H	-3.31499	-2.75045	1.23662
H	2.75046	3.31499	-1.23661
H	4.77598	3.40544	-2.63094
H	4.77597	-3.40544	-2.63096
H	2.75045	-3.31499	-1.23662
H	-2.75046	-3.31499	-1.23661
H	-4.77598	-3.40544	-2.63094
H	-4.77597	3.40544	-2.63096
H	-2.75045	3.31499	-1.23662

Table S7. Atom coordinates of optimized structure of **T-CN**$^{2-}$ (charge –2, multiplicity 3).

atom	x	y	z
C	-1.64797	0.63367	0.3415
C	-0.63097	1.59662	0.36517
C	-2.7725	1.13841	1.14342
C	-3.99635	0.62065	1.54707
C	-4.81269	1.40061	2.37845
C	-4.44128	2.67317	2.84457
C	-1.08214	2.71708	1.17522
C	-2.39219	2.41117	1.63876
C	-3.16386	3.2165	2.48103
C	-2.55519	4.46153	2.87134
C	-1.26067	4.76684	2.41425
C	-0.51347	3.92133	1.58466
C	3.99635	-0.62065	1.54707
C	4.81269	-1.40061	2.37845
C	4.44128	-2.67317	2.84457
C	3.16386	-3.2165	2.48103
C	2.39219	-2.41117	1.63876
C	2.7725	-1.13841	1.14342
C	2.55519	-4.46153	2.87134
C	1.26067	-4.76684	2.41425
C	0.51347	-3.92133	1.58466
C	1.08214	-2.71708	1.17522
C	1.64797	-0.63367	0.3415
C	0.63097	-1.59662	0.36517
C	0.51345	3.9213	-1.58473
C	1.26066	4.76681	-2.41432
C	2.55519	4.46152	-2.87138
C	3.16387	3.2165	-2.48103
C	2.3922	2.41117	-1.63877
C	1.08214	2.71706	-1.17526
C	4.44131	2.67318	-2.84453
C	4.81273	1.40064	-2.37838
C	3.99639	0.62068	-1.54701
C	2.77251	1.13842	-1.14339
C	0.63096	1.59661	-0.36519
C	1.64797	0.63367	-0.34149
C	-0.63096	-1.59661	-0.36519
C	-1.64797	-0.63367	-0.34149
C	-1.08214	-2.71706	-1.17526
C	-0.51345	-3.9213	-1.58473
C	-1.26066	-4.76681	-2.41432
C	-2.55519	-4.46152	-2.87138
C	-2.77251	-1.13842	-1.14339
C	-2.3922	-2.41117	-1.63877
C	-3.16387	-3.2165	-2.48103
C	-4.44131	-2.67318	-2.84453
C	-4.81273	-1.40064	-2.37838
C	-3.99639	-0.62068	-1.54701
C	-3.18342	5.41671	3.7149
N	-3.62778	6.24524	4.39279
C	-5.38031	-3.34964	-3.6736
N	-6.20101	-3.83047	-4.33435
C	5.38031	3.34964	-3.6736
N	6.20101	3.83047	-4.33435
C	3.18342	-5.41671	3.7149
N	3.62778	-6.24524	4.39279
C	-3.18342	-5.41669	-3.71494
N	-3.62778	-6.24521	-4.39285
C	5.38027	-3.34963	3.67366
N	6.20096	-3.83044	4.33442
C	3.18342	5.41669	-3.71494
N	3.62778	6.24521	-4.39285
C	-5.38027	3.34963	3.67366
N	-6.20096	3.83044	4.33442
H	-4.32949	-0.36157	1.23724
H	-5.7767	1.0134	2.68577
H	-0.82545	5.70563	2.73611
H	0.48549	4.20888	1.28291

H	4.32949	0.36157	1.23724
H	5.7767	-1.0134	2.68577
H	0.82545	-5.70563	2.73611
H	-0.48549	-4.20888	1.28291
H	-0.48551	4.20884	-1.283
H	0.82543	5.70559	-2.7362
H	5.77675	1.01344	-2.68567
H	4.32954	-0.36153	-1.23716
H	0.48551	-4.20884	-1.283
H	-0.82543	-5.70559	-2.7362
H	-5.77675	-1.01344	-2.68567
H	-4.32954	0.36153	-1.23716

Table S8. Atom coordinates of optimized structure of **T** (charge 0, multiplicity 1).

atom	x	y	z
C	0.60457	-1.60975	-0.37127
C	1.59279	-0.64765	-0.37168
C	1.04849	-2.73912	-1.2178
C	0.49911	-3.9348	-1.63039
C	1.25341	-4.76443	-2.50728
C	2.50644	-4.41148	-2.97313
C	2.70943	-1.12193	-1.21861
C	2.32859	-2.39256	-1.70635
C	3.08748	-3.17243	-2.57838
C	4.34134	-2.6248	-2.97415
C	4.72781	-1.38139	-2.50914
C	3.91909	-0.60481	-1.63217
C	-0.49911	3.9348	-1.63039
C	-1.25341	4.76443	-2.50728
C	-2.50644	4.41148	-2.97313
C	-3.08748	3.17243	-2.57838
C	-2.32859	2.39256	-1.70635
C	-1.04849	2.73912	-1.2178
C	-4.34134	2.6248	-2.97415
C	-4.72781	1.38139	-2.50914
C	-3.91909	0.60481	-1.63217
C	-2.70943	1.12193	-1.21861
C	-0.60457	1.60975	-0.37127
C	-1.59279	0.64765	-0.37168
C	3.93482	0.49911	1.63036
C	4.76445	1.25341	2.50725
C	4.41149	2.50644	2.97312
C	3.17243	3.08747	2.57838
C	2.39256	2.32859	1.70635
C	2.73912	1.04849	1.21779
C	2.6248	4.34133	2.97416
C	1.38138	4.7278	2.50917
C	0.6048	3.91908	1.63219
C	1.12192	2.70943	1.21862
C	1.60975	0.60457	0.37128
C	0.64765	1.59279	0.37168
C	-1.60975	-0.60457	0.37128
C	-0.64765	-1.59279	0.37168
C	-2.73912	-1.04849	1.21779
C	-3.93482	-0.49911	1.63036
C	-4.76445	-1.25341	2.50725
C	-4.41149	-2.50644	2.97312
C	-1.12192	-2.70943	1.21862
C	-2.39256	-2.32859	1.70635
C	-3.17243	-3.08747	2.57838
C	-2.6248	-4.34133	2.97416
C	-1.38138	-4.7278	2.50917
C	-0.6048	-3.91908	1.6322
H	-0.48622	-4.25042	-1.30908
H	0.82006	-5.70604	-2.82472
H	3.04264	-5.0727	-3.64496
H	4.98765	-3.17876	-3.64607
H	5.68045	-0.97344	-2.82734
H	4.26112	0.37188	-1.31147
H	0.48622	4.25042	-1.30908
H	-0.82006	5.70604	-2.82472
H	-3.04264	5.0727	-3.64496
H	-4.98765	3.17876	-3.64607
H	-5.68045	0.97344	-2.82734
H	-4.26112	-0.37188	-1.31147
H	4.25043	-0.48621	1.30904
H	5.70606	0.82007	2.82468
H	5.07271	3.04264	3.64494
H	3.17876	4.98764	3.64609
H	0.97343	5.68042	2.82739
H	-0.37189	4.2611	1.31151
H	-4.25043	0.48621	1.30904
H	-5.70606	-0.82007	2.82468
H	-5.07271	-3.04264	3.64494
H	-3.17876	-4.98764	3.64609
H	-0.97343	-5.68042	2.82739

H	0.37189	-4.2611	1.31151

11. Calculated Steady State Absorption Spectra

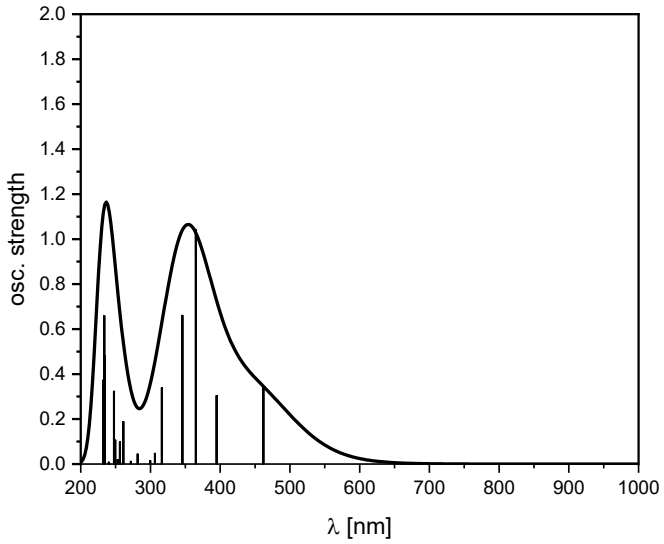

Figure S34. Calculated steady-state absorption spectrum of **T-CN** (TD, CAM-B3LYP(D3BJ)/6-311+G(d,p), PCM (CH_2Cl_2)). The simulated spectrum was broadened using Gaussian function and full width at half maximum set to 0.20 eV.

Table S9. Vertical excitations of **T-CN** (TD, CAM-B3LYP(D3BJ)/6-311+G(d,p), PCM (CH_2Cl_2)). Only the contributions with largest linear response coefficients (in parentheses) are shown.

Excitation	*E* [eV]	λ [nm]	Type	F
S_1	1.97	629	HOMO → LUMO (0.68)	0.0
S_2	2.68	462	HOMO → LUMO+1 (0.46)	0.34
S_3	2.68	462	HOMO → LUMO+2 (0.46)	0.34
S_4	2.80	442	HOMO → LUMO+3 (0.59)	0.0
S_5	3.14	394	HOMO–2 → LUMO (0.53)	0.30
S_6	3.14	394	HOMO–1 → LUMO (0.53)	0.30
S_7	3.40	365	HOMO–3 → LUMO (0.49)	1.04
S_8	3.53	351	HOMO–1 → LUMO+2 (0.31)	0.0
S_9	3.58	346	HOMO–6 → LUMO (0.38)	0.66
S_{10}	3.58	346	HOMO–1 → LUMO+3 (0.33)	0.66

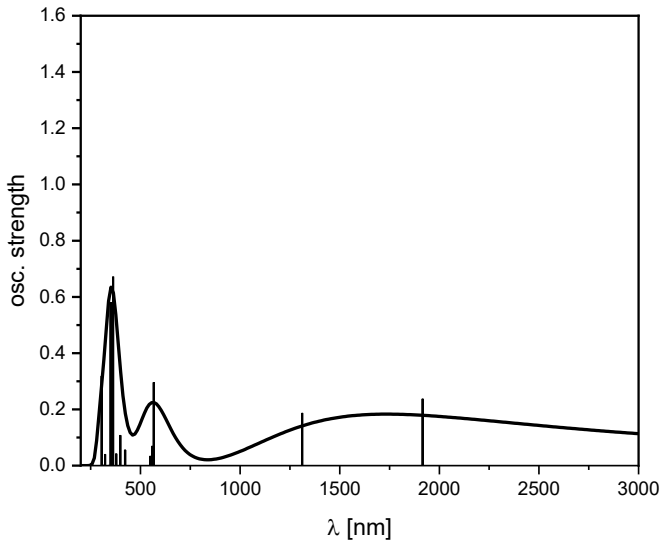

Figure S35. Calculated steady-state absorption spectrum of **T-CN**$^{\bullet-}$ (TD, CAM-B3LYP(D3BJ)/6-311+G(d,p), PCM (THF). The simulated spectrum was broadened using Gaussian function and full width at half maximum set to 0.20 eV.

Table S10. Vertical excitations of **T-CN**$^{\bullet-}$ (TD, CAM-B3LYP(D3BJ)/6-311+G(d,p), PCM (THF)). Only the contributions with largest linear response coefficients (in parentheses) are shown.

Excitation	*E* [eV]	λ [nm]	Type	F
D_1	0.65	1916	αHOMO → αLUMO+1 (0.87)	0.24
D_2	0.65	1916	αHOMO → αLUMO (0.87)	0.24
D_3	0.95	1312	αHOMO → αLUMO+2 (0.98)	0.19
D_4	1.19	1043	βHOMO-1 → βHOMO (0.91)	0.0
D_5	1.60	775	αHOMO–1 → αLUMO (0.70)	0.0
D_6	1.60	775	αHOMO–1 → αLUMO+1 (0.70)	0.0
D_7	1.86	668	αHOMO–1 → αLUMO+2 (0.67)	0.0
D_8	2.19	567	αHOMO–1 → αLUMO (0.42)	0.30
D_9	2.19	567	αHOMO–1 → αLUMO+1 (0.42)	0.30
D_{10}	2.19	567	βHOMO–5 → βHOMO (0.37)	0.0

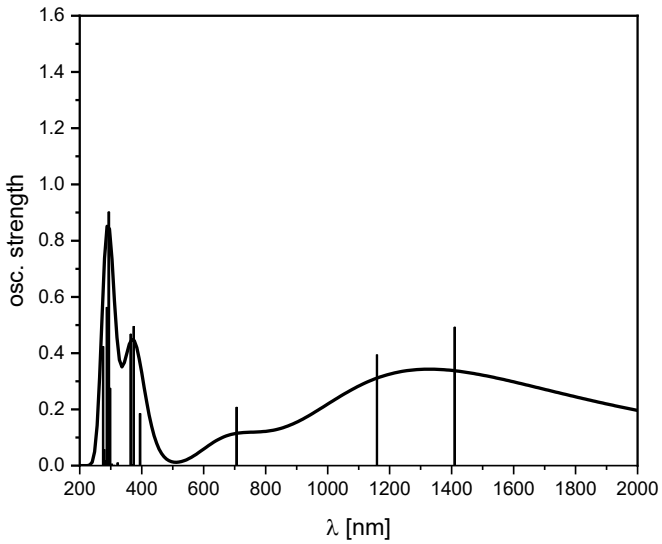

Figure S36. Calculated steady-state absorption spectrum of **T-CN**$^{2-}$ (TD, CAM-B3LYP(D3BJ)/6-311+G(d,p), PCM (THF), singlet state). The simulated spectrum was broadened using Gaussian function and full width at half maximum set to 0.20 eV.

Table S11. Vertical excitations of **T-CN**$^{2-}$ (TD, CAM-B3LYP(D3BJ)/6-311+G(d,p), PCM (THF), singlet state). Only the contributions with largest linear response coefficients (in parentheses) are shown.

Excitation	*E* [eV]	λ [nm]	Type	f
S_1	0.88	1410	HOMO → LUMO+1 (0.69)	0.49
S_2	0.88	1410	HOMO → LUMO (0.69)	0.49
S_3	1.07	1159	HOMO → LUMO+2 (0.70)	0.39
S_4	1.76	706	HOMO–1 → LUMO (0.67)	0.21
S_5	1.76	706	HOMO–1 → LUMO+1 (0.67)	0.21
S_6	1.90	653	HOMO–1 → LUMO+2 (0.67)	0.0
S_7	2.95	420	HOMO–2 → LUMO (0.35)	0.0
S_8	2.97	417	HOMO → LUMO+3 (0.62)	0.0
S_9	3.14	395	HOMO → LUMO+5 (0.57)	0.19
S_{10}	3.14	395	HOMO → LUMO+6 (0.57)	0.19

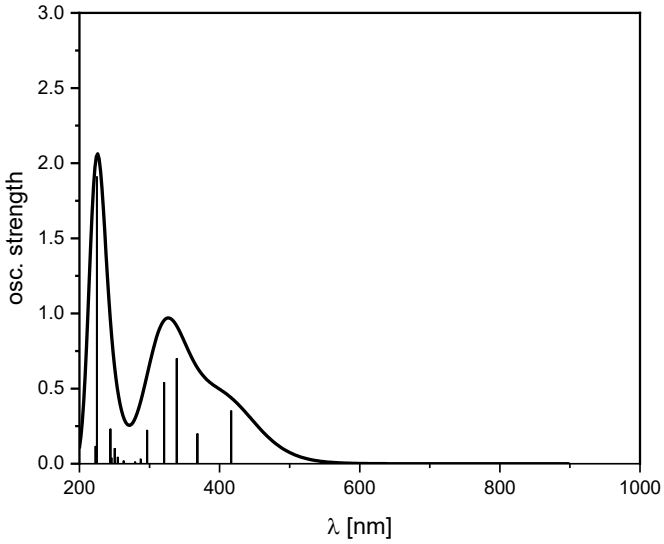

Figure S37. Calculated steady-state absorption spectrum of **T** (TD, CAM-B3LYP(D3BJ)/6-311+G(d,p), PCM (CH_2Cl_2)). The simulated spectrum was broadened using Gaussian function and full width at half maximum set to 0.20 eV.

Table S12. Vertical excitations of **T** (TD, CAM-B3LYP(D3BJ)/6-311+G(d,p), PCM (CH_2Cl_2)). Only the contributions with largest linear response coefficients (in parentheses) are shown.

Excitation	*E* [eV]	λ [nm]	Type	F
S_1	2.17	572	HOMO → LUMO (0.68)	0.0
S_2	2.98	417	HOMO → LUMO+1 (0.55)	0.35
S_3	2.98	417	HOMO → LUMO+2 (0.55)	0.35
S_4	3.12	397	HOMO → LUMO+3 (0.59)	0.0
S_5	3.37	368	HOMO–1 → LUMO (0.57)	0.20
S_6	3.37	368	HOMO–2 → LUMO (0.57)	0.20
S_7	3.66	339	HOMO–3 → LUMO (0.52)	0.70
S_8	3.80	326	HOMO–1 → LUMO+1 (0.32)	0.0
S_9	3.86	321	HOMO–5 → LUMO (0.44)	0.54
S_{10}	3.86	321	HOMO–6 → LUMO (0.44)	0.54

12. Electrostatic Potential Maps

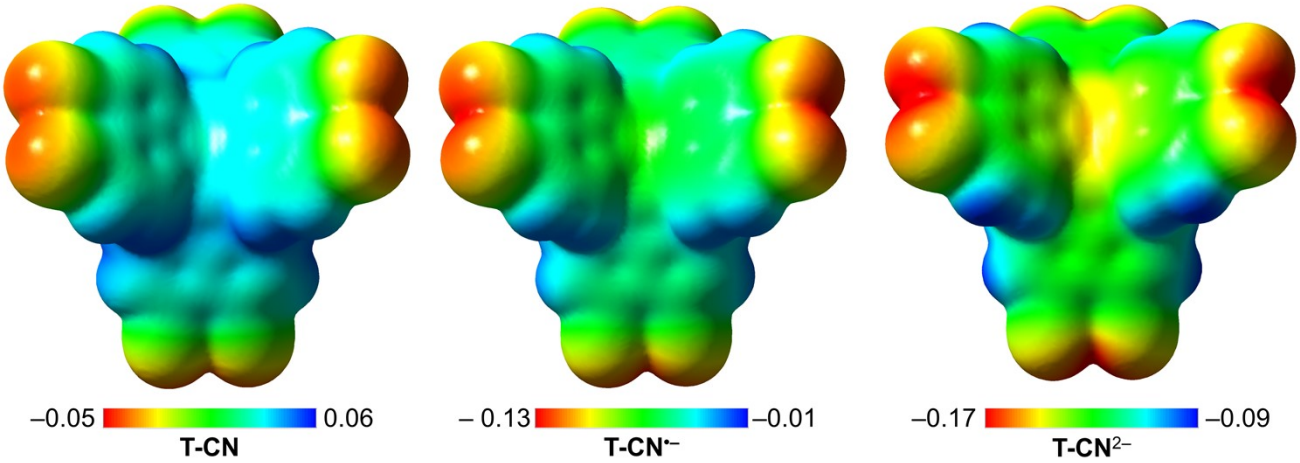

Figure S38. Electrostatic potential mapped onto the electron density for **T-CN**, **T-CN$^{\bullet-}$** and **T-CN^{2-}** (singlet state)**.**

13. Calculated Spin Density of T-CN$^{\bullet-}$

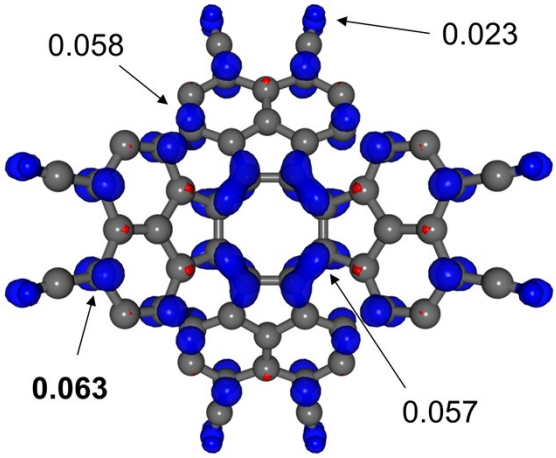

Figure S39. Calculated spin density map of **T-CN$^{\bullet-}$** (B3LYP(D3BJ)/6-311+G(d,p) and Mulliken spin population values for selected atoms.

14. NICS Values

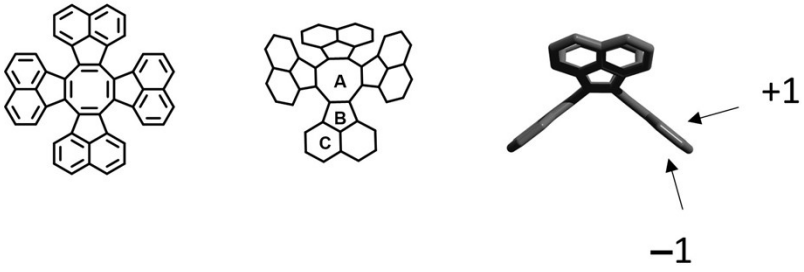

Table S13. NICS values of **T** at the B3LYP(D3BJ)/6-311+G(d,p) level of theory.

T	A	B	C
NICS (–1)	+2.25	+1.66	–8.91
NICS (+1)	+2.25	+0.83	–8.31
$NICS(-1)_{zz}$	+18.5	+8.38	–23.2
$NICS(+1)_{zz}$	+18.5	+6.34	–22.3
$NICS(1)_{zz\text{-}av}$	+18.5	+7.36	–22.8

Table S14. NICS values of **T-CN** at the B3LYP(D3BJ)/6-311+G(d,p) level of theory.

T-CN	**A**	**B**	**C**
NICS (–1)	+1.78	+1.85	–8.78
NICS (+1)	+1.78	+1.10	–8.18
$NICS(-1)_{zz}$	+17.1	+9.66	–21.0
$NICS(+1)_{zz}$	+17.1	+7.70	–20.1
$NICS(1)_{zz\text{-}av}$	+17.1	+8.68	–20.6

15. HOMA Values

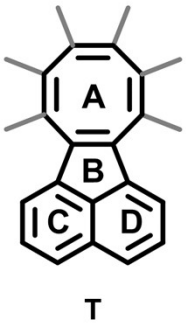

T

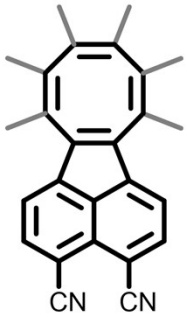

T-CN

Table S15. HOMA values of **T** and **T-CN** calculated from the X-ray crystal structure and the DFT-optimized geometries calculated at the B3LYP(D3BJ)/6-311+G(d,p) level of theory. The X-ray crystal structure of **T** was obtained from the Cambridge Structural Database.[17]

Ring	T X-ray	T DFT	T-CN X-ray	T-CN DFT
A	+0.19	+0.39	+0.20	+0.41
B	+0.09	+0.07	+0.09	+0.11
C	+0.87	+0.86	+0.85	+0.83
D	+0.88	+0.86	+0.86	+0.83

16. References

1 G. R. Fulmer, A. J. M. Miller, N. H. Sherden, H. E. Gottlieb, A. Nudelman, B. M. Stoltz, J. E. Bercaw and K. I. Goldberg, *Organometallics*, 2010, **29**, 2176–2179.

2 G. M. Sheldrick, *Acta Crystallogr., Sect. A: Found. Crystallogr.* 2008, **64**, 112–122.

3 G. M. Sheldrick, *Acta Crystallogr., Sect. C: Cryst. Struct. Commun.* 2015, **71**, 3–8.

4 C. F. Macrae, P. R. Edgington, P. McCabe, E. Pidcock, G. P. Shields, R. Taylor, M. Towler and J. van de Streek, *J. Appl. Crystallogr.* 2015, **39**, 453–457.

5 M. Krejčik, M. Daněk and F. Hartl, *J. Electroanal. Chem. Interf. Electrochem.*, 1991, **317**, 179–187.

6 M. J. Frisch, G. W. Trucks, H. B. Schlegel, G. E. Scuseria, M. A. Robb, J. R. Cheeseman, G. Scalmani, V. Barone, G. A. Petersson, H. Nakatsuji, X. Li, M. Caricato, A. V. Marenich, J. Bloino, B. G. Janesko, R. Gomperts, B. Mennucci, H. P. Hratchian, J. V. Ortiz, A. F. Izmaylov, J. L. Sonnenberg, Williams, F. Ding, F. Lipparini, F. Egidi, J. Goings, B. Peng, A. Petrone, T. Henderson, D. Ranasinghe, V. G. Zakrzewski, J. Gao, N. Rega, G. Zheng, W. Liang, M. Hada, M. Ehara, K. Toyota, R. Fukuda, J. Hasegawa, M. Ishida, T. Nakajima, Y. Honda, O. Kitao, H. Nakai, T. Vreven, K. Throssell, J. A. Montgomery Jr., J. E. Peralta, F. Ogliaro, M. J. Bearpark, J. J. Heyd, E. N. Brothers, K. N. Kudin, V. N. Staroverov, T. A. Keith, R. Kobayashi, J. Normand, K. Raghavachari, A. P. Rendell, J. C. Burant, S. S. Iyengar, J. Tomasi, M. Cossi, J. M. Millam, M. Klene, C. Adamo, R. Cammi, J. W. Ochterski, R. L. Martin, K. Morokuma, O. Farkas, J. B. Foresman and D. J. Fox, *Gaussian 16 Rev. C.01*, Wallingford, CT, 2016.

7 a) P. J. Stephens, F. J. Devlin, C. F. Chabalowski and M. J. Frisch, *J. Phys. Chem.* 1994, **98**, 11623–11627; b) A. D. Becke, *J. Chem. Phys.* 1993, **98**, 5648–5652; c) Lee, Yang, Parr, *Phys. Rev. B Condens. Matter* 1988, **37**, 785–789; d) S. H. Vosko, L. Wilk and M. Nusair, *Can. J. Phys.* 1980, **58**, 1200–1211.

8 a) T. Clark, J. Chandrasekhar, G. W. Spitznagel and P. V. R. Schleyer, *J. Comput. Chem.* 1983, **4**, 294–301; b) R. Krishnan, J. S. Binkley, R. Seeger and J. A. Pople, *J. Chem. Phys.* 1980, **72**, 650–654.

9 S. Grimme, J. Antony, S. Ehrlich and H. Krieg, *J. Chem. Phys.* 2010, **132**, 154104.

10 S. Grimme, S. Ehrlich and L. Goerigk, *J. Comput. Chem*. 2011, **32**, 1456–1465.

11 Takeshi Yanai, David P. Tew and Nicholas C. Handy, *Chem. Phys. Lett.* 2004, **393**, 51–57.

12 a) M. Cossi, N. Rega, G. Scalmani and V. Barone, *J. Comput. Chem.* 2003, **24**, 669–681; b) V. Barone and M. Cossi, *J. Phys. Chem. A* 1998, **102**, 1995–2001.

13 Roy Dennington, Todd A. Keith and John M. Millam, *GaussView Version 6*, 2019.

14 J. R. Cheeseman, G. W. Trucks, T. A. Keith and M. J. Frisch, *J. Chem. Phys.* 1996, **104**, 5497–5509.

15 a) K. Wolinski, J. F. Hinton and P. Pulay, *J. Am. Chem. Soc.* 1990, **112**, 8251–8260; b) R. Ditchfield, *Mol. Phys.* 1974, **27**, 789–807; c) R. McWeeny, *Phys. Rev.* 1962, **126**, 1028–1034; d) F. London, *J. Phys. Radium* 1937, **8**, 397–409.

16 T. Lu and F. Chen, *J. Comput. Chem.* 2012, **33**, 580–592.

17 W. D. Neudorff, D. Lentz, M. Anibarro and A. D. Schlüter, *Chem. Eur. J.*, 2003, **9**, 2745–2757.

18 D. P. Sumy, N. J. Dodge, C. M. Harrison, A. D. Finke and A. C. Whalley, *Chem. Eur. J.*, 2016, **22**, 4709–4712.